Wearable Pressure Sensor Suit for Real-Time Detection of Incorrect Exercise Techniques

Thesis submitted in partial fulfillment
of the requirements for the degree of

Master of Science in ***Electronics and Communication Engineering*** *by Research*

by

Ivin Kuriakose
2019112018
ivin.kuriakose@research.iiit.ac.in

International Institute of Information Technology
Hyderabad - 500 032, INDIA
June 2024

International Institute of Information Technology

Hyderabad, India

CERTIFICATE

It is certified that the work contained in this thesis, titled **"Wearable Pressure Sensor Suit for Real-Time Detection of Incorrect Exercise Techniques"** by Ivin Kuriakose, has been carried out under my supervision and is not submitted elsewhere for a degree.

Date	Adviser: Dr. Aftab M Hussain

To getting closer to the dreams I wake up to

Acknowledgments

This acknowledgment goes to my incredible friends and family that has made my life happier. I would like to thank everybody who has made my college life more memorable, my batchmates, my seniors, and my juniors. Firstly, thank my mom, dad, and sister for making my college life so smooth and helping me financially. Next, to my friends who made every day so joyful. Pratishtha Abrol thank you for pushing me to my limits when I needed it and sorting mails. Your support was immense throughout this journey. Rhuthik, Vivek, pranoy, sivaprasad, Rahul, and everybody in the Mallu gang, every day was so eventful with you guys around. Ashish Gupta and everybody in the fifth-floor gang, thank you so much. I will always cherish the memories we made throughout our college life.

Next, I would love to express my gratitude to my lab mates in the PATRIoT+FleCS lab without whom research might not have been this fun and successful. Firstly I thank Shirley Chauhan, who did the data analysis part of this research. Thank you for your constant assistance and support, academically and non-academically. A big thanks to my colleagues Anis Fatema, Kirthi Vignan, Nitheesh, Mohee Datta Gupta, Chetanya Goyal, and everybody else. I learned everything from you guys and I will always be indebted.

Lastly, the biggest thank you to my advisor, Dr. Aftab Hussain for the trust he put in me. Thank you for the freedom you gave me, to choose what I wanted to do and explore new things. I am heavily indebted to you for everything.

Abstract

In recent times, the popularity of gym culture has witnessed a remarkable surge. The pursuit of a healthier lifestyle, increased awareness of the benefits of regular exercise, and the desire for physical well-being have contributed to the widespread embrace of gym activities. Individuals across diverse age groups and backgrounds are increasingly recognizing the importance of incorporating fitness into their daily routines, leading to a higher interest in gym memberships and fitness classes.

One crucial aspect of effective workouts is the importance of exercise form. Whether engaging in weightlifting, cardio exercises, flexibility routines, or even yoga, the proper execution of movements is crucial for maximizing benefits and preventing injuries. Maintaining correct posture, alignment, and technique not only enhances the efficiency of the workout but also safeguards against potential strains and stresses on the body.

Recognizing the significance of exercise form, there is a growing demand for innovative solutions that can assist individuals in ensuring they perform exercises correctly. The need for a device that checks and monitors one's form has become evident in the fitness landscape. This thesis presents a suit that provides real-time feedback, offering guidance on posture, movement range, and overall form during exercises. By integrating this technology into the fitness routine, individuals can optimize their workouts, reduce the risk of injuries, and enhance the overall effectiveness of their training sessions.

This innovative suit employs pressure sensors to precisely calculate the flexion of individual muscle groups, thereby assessing the form of exercise. Utilizing piezo-resistive material, namely velostat, for our pressure sensors ensures dynamic responsiveness. The resistance varies proportionally based on the degree of muscle stretching, enabling the identification of over-stretching or under-stretching that may indicate suboptimal form. By comprehensively analyzing data from all sensors, we can accurately evaluate the proficiency of the exercise form.

The focus of this thesis centers on a specialized suit designed to analyze the form of the back muscles during various exercises such as squats, deadlifts, and rows. The suit incorporates multiple sensors

strategically placed on the back, seamlessly connected to the ESP32 microcontroller. This setup enables real-time feedback, with all necessary calculations performed on the microcontroller itself. Notably, the suit prioritizes user comfort by offering flexibility and durability without any rigid components that might impede the workout experience. Additionally, the suit features a detachable battery, ensuring its complete washability.

Impressively, our suit demonstrates an accuracy range of 72% to 90% across the three specified exercises, highlighting its efficacy in precisely evaluating exercise form. This research not only contributes to the growing field of wearable technology in fitness but also underscores the potential for real-time, personalized feedback to enhance users' workout experiences.

Contents

List of Figures

List of Tables

Chapter 1

Introduction

Physical fitness has gained unprecedented significance in contemporary society, with weight training emerging as a cornerstone for muscle development[1], weight management[2], and overall body enhancement. Central to weight training is the principle of progressive overload, emphasizing the systematic increase in resistance to stimulate muscle growth[3]. However, achieving optimal results requires not only dedication but also a keen focus on proper form and technique during exercises. The significance of maintaining correct body posture while engaging in weightlifting cannot be overstated, as it not only maximizes the benefits of the workout but also plays a crucial role in preventing injuries[4].

Despite the acknowledged importance of correct form, a significant challenge exists for individuals undertaking weight training – the lack of access to qualified instructors who can monitor and guide them in real-time. This limitation is particularly worrying in exercises such as the deadlift and squat, compound movement targeting multiple muscle groups simultaneously, including the lower back, legs, and core[5, 6]. Unfortunately, these exercises are notorious for their potential to cause injuries, ranging from muscular strains to more severe complications affecting the spine, hips, and knees[7, 8, 9, 10]. Even the most experienced powerlifters face potential risks, as evidenced by a study involving 104 expert powerlifters. Surprisingly, 31% reported injuries during deadlifts, while a staggering 43% experienced injuries during squat training[11]. This heightened risk is attributed to the demanding nature of these powerful lifts, where heavy weights are inherently part of the training. Thus, there is a pressing need for innovative solutions that can address the dual challenge of optimizing exercise form and minimizing injury risks. In response to this challenge, the fitness landscape has witnessed a surge in the use of technology to aid individuals in monitoring their exercise routines.

This research thesis introduces a groundbreaking approach to real-time form assessment during weight training through the development of a wearable pressure sensor suit. Leveraging the innovative concept of piezoresistivity[12], our suit utilizes a flexible material known as velostat [13], ensuring adaptability to various body shapes and exercise modalities. The primary objective of this research is to offer an accessible, user-friendly, and effective solution for individuals seeking to optimize their exercise form and mitigate the risks of injuries. The suit integrates seamlessly into the workout routine, providing instant feedback on posture and form through a detachable microcontroller and a Bluetooth-enabled connection to a mobile phone. Moreover, this technology is not only flexible and washable but also cost-effective, addressing the current gaps in existing methodologies.

As we delve into the subsequent sections of this thesis, we will explore the theoretical underpinnings of piezoresistivity, the development and design of the pressure sensor suit, its integration with real-time processing units, and the results of empirical testing. Through this research, we aim to contribute to the evolving landscape of wearable technology in the fitness domain, offering a novel solution that combines technological innovation with practical utility.

1.1 Thesis Layout

The thesis is organized as follows:

- **Chapter 1:** In this chapter, we discuss the prerequisites or background work that is necessary to understand the work presented in later chapters. The chapter gives a brief introduction to the research and states the contribution of each member.

- **Chapter 2:** In this chapter, we discuss the current scenario and available solutions. We also look into few researches in similar domain, and discuss how our research differs from it.

- **Chapter 3:** In this chapter, we discuss the design and architecture of the suit. The chapter goes into detail about the requirements and each component of the suit. Discussion about the pressure sensors, the different types of pressure sensors, their working principles, etc. is also done here.

- **Chapter 4:** This chapter explains the experiments and their corresponding result. The section explains the exercises we will be analyzing and the precautions taken during the data collection. Then we go into the details of both experiments.

- **Chapter 5:** In this chapter, we conclude with a summary of the methods and results discussed in this thesis.

Chapter 2

Literature Review

2.1 Video on Demand

Video-on-demand (VOD) platforms have become a popular choice, with 44% of gym-goers incorporating them into their weekly workout routines[14]. However, while VOD platforms offer valuable visual instruction, they lack the immediacy and interactivity required for real-time corrections during weightlifting sessions. Moreover, these platforms often fall short of providing comprehensive assessments, particularly in cases where equipment is limited and environmental factors may compromise their effectiveness. Research by Sokolova et. al.[15] discusses the intentions and consistency of people who watch fitness-related content on YouTube. It also, talks about the effectiveness of posture correction. Vancini et.al [16] also discuss the limitation of using video clips for workout form.

2.2 Computer Vision

Posture detection through computer vision has emerged as a notably effective method for identifying improper exercise posture with a high level of accuracy 2.2[17]. This sophisticated technique involves meticulously calculating distances and angles between key anatomical points such as the back, knee, and the loaded weight, providing users with valuable feedback [18]. This technique has its own major setbacks. One significant limitation arises from the requirement for specialized equipment and the need for meticulously optimized scene settings. This specialized setup implies that these techniques may not be seamlessly integrated into public gym environments, which are usually crowded and diverse.

The drawbacks include a limited capture zone, which will restrict the system's ability to monitor users across different workout areas comprehensively. Moreover, the presence of various reflective surfaces

((a)) Exercise form check using IMU sensor[19]

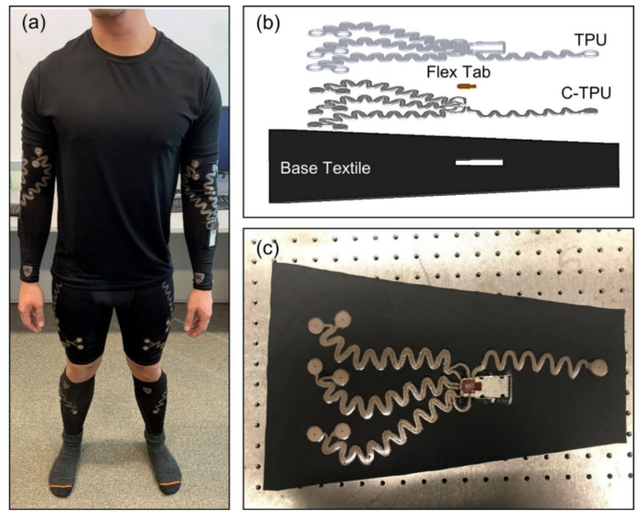

((b)) Exercise form check using sEMG device[20]

Figure 2.1: Wearable Exercise Correction device

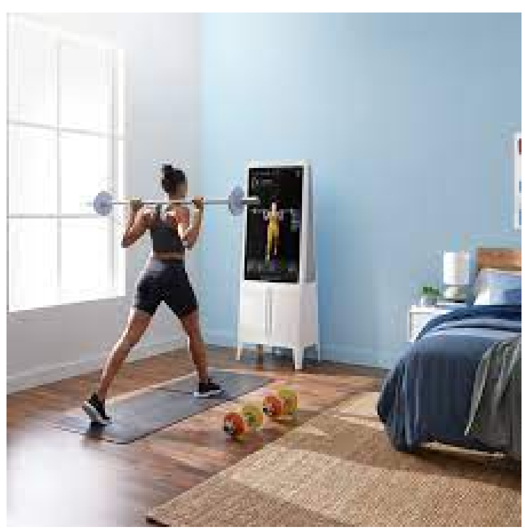

Figure 2.2: Exercise form check using computer vision[17]

and objects in a gym setting introduces the risk of marker occlusions, hindering the accurate tracking of key points during exercises. The effectiveness of this techniques peaks in a controlled environment, which means their seamless integration into public gym spaces challenging [21].

2.3 Wearble suit using sEMG and IMU sensors

Various wearable methods have been explored for real-time form detection, and among them are devices incorporating Inertial Measurement Unit (IMU) sensors or surface electromyography (sEMG) sensors [20, 22, 23]. A noteworthy approach by Michaud et al. involves the utilization of a 9-degree-of-freedom (9-DOF) IMU sensor 2.1(a), adept at approximating the intricate motion of multiple joints in three-dimensional space to assess the correctness of exercise posture [21]. However, it is crucial to acknowledge that IMU sensors, despite their capabilities, exhibit susceptibility to drift, even with meticulous offset elimination through magnetometers [19]. This inherent limitation necessitates frequent recalibration to maintain optimal accuracy, adding a layer of complexity to their practical deployment in real-world scenarios. Furthermore, the rigid nature of IMU sensors renders them less suitable for exercises such as bench presses and various seated exercises where the load is positioned directly atop the sensor, compromising their versatility across a spectrum of workout routines.

In a parallel trajectory, alternative investigations by Wang et al. and Hannan et al. delve into the realm of sEMG sensors for real-time form detection 2.1(b) [20, 24]. These sensors aim to capture muscle fiber activity across various muscle groups as a means of discerning and evaluating exercise posture. Yet, this process comes with its own set of challenges. The intricate nature of the electromyography (EMG) signal poses a formidable hurdle in accurately representing posture and spinal dynamics. Achieving a comprehensive understanding of exercise form based on muscle fiber activity alone remains a complex task, which needs further exploration and refinement of methodologies [25].

2.4 Posture detection for domains outside gym

Research by Yang et al. [26] delves into the use of wearable sensor suits for posture detection and correction, focusing specifically on neutral standing and sitting positions. The study highlights how sensor suits equipped with accelerometers and gyroscopes can monitor the angles and movements of different body parts. The data collected from these sensors are then processed to determine deviations from neutral postures, enabling real-time feedback and corrections. This approach is particularly beneficial in ergonomic applications, where maintaining proper posture can prevent musculoskeletal disorders.

Nagarkoti et al. [27] explores real-time posture analysis during indoor workouts using machine learning and computer vision techniques. The paper primarily focuses on yoga and other bodyweight exercises. By employing convolutional neural networks (CNNs) to process video data, the system can identify and evaluate various poses. The research emphasizes the importance of accurate posture detection in exercise routines to ensure correct form, which is crucial for effectiveness and injury prevention. This method leverages the accessibility of cameras and the computational power of modern processors to provide a cost-effective solution for posture monitoring.

Ze Wu et al. [28] investigate the use of Inertial Measurement Unit (IMU) sensors for recognizing and quantitatively evaluating yoga postures. IMU sensors, which include accelerometers, gyroscopes, and magnetometers, are attached to key body parts to capture detailed motion data. The collected data is processed on a high-capability device using a back-propagation artificial neural network (ANN) to classify different yoga poses and assess their quality. This research highlights the precision of IMU sensors in capturing subtle movements and the effectiveness of ANNs in interpreting complex motion data, making it a robust solution for posture detection in controlled environments.

In the study conducted by Xiaoou et al. [29], the authors present a method for human posture detection using wearable suits equipped with surface electromyography (sEMG) sensors. These sensors measure muscle activity, providing insights into the movements associated with different postures. The research evaluates normal human movements such as standing, sitting, and bending using Support Vector Machine (SVM) models to classify the data. This method not only captures the posture but also offers a deeper understanding of the muscular engagement involved, making it valuable for both medical and athletic applications.

Nadeem et al. [30] employ computer vision techniques to evaluate posture during sports activities, specifically tennis and football. The study utilizes video analysis to capture and assess the movements of athletes, ensuring that their posture aligns with optimal performance standards. By using algorithms that can detect and track body parts, the system provides real-time feedback on posture, helping athletes to improve their form and reduce the risk of injuries. This approach demonstrates the potential of computer vision in enhancing athletic performance through detailed posture analysis.

Chapter 3

Design Process and Architecture of Suit

3.1 Introduction

The design and selection of components play a pivotal role in the development of the suit. Every aspect of the suit, from its structural elements to the embedded technology, contributes to its effectiveness and user experience. Firstly, the design of the suit must prioritize comfort and flexibility to ensure a seamless integration into the user's workout routine. A well-thought-out design considers the body's natural movements, minimizing restrictions while providing necessary support to enhance performance. The choice of components, such as sensors and data processing units, is equally crucial. High-quality sensors embedded strategically in the suit can accurately capture biomechanical data, enabling precise form analysis. Selecting advanced data processing components ensures real-time feedback, allowing users to make instant corrections and optimize their workout sessions. In this chapter, we will design the suit step-by-step. We will first discuss the requirements a user expects from the suit and then we will discuss each component and why it was chosen in detail.

3.2 Requirements for the suit

In pursuit of crafting an innovative exercise suit tailored for the everyday gym enthusiast, our primary objective is to ensure optimal comfort throughout the entire exercise routine, from wearing to washing. The envisioned wearable must be user-friendly, allowing individuals to effortlessly put it on without the need for external assistance. This ease of donning is not merely a convenience but an essential aspect of the user experience, promoting independence and efficiency.

Emphasizing the importance of comfort during workouts, the exercise suit should not impede the natural movements and performance of the user. A key facet of this is the suit's weight – it must be lightweight to facilitate unhindered movement and agility. Additionally, recognizing the inevitability of perspiration during intense workouts, the suit needs to be equipped with sweat-resistant materials. A critical consideration here is safeguarding any embedded electronics or metallic components from direct exposure to sweat, as sweat-induced corrosion could compromise the durability and functionality of the suit over time.

Striking a delicate balance between flexibility and power consumption is imperative for the success of the exercise suit. Maximum flexibility ensures that the user can seamlessly engage in a diverse range of exercises without any constraints. Simultaneously, minimizing power requirements is crucial to prevent the inconvenience of a bulky battery hindering the user's overall gym experience.

Furthermore, the design philosophy of the exercise suit states the exclusion of rigid components. This decision serves a dual purpose: firstly, to enhance the suit's resilience by eliminating vulnerable points of potential damage, and secondly, to ensure the suit doesn't interfere with exercises that require the user to be in a certain position. The absence of rigid parts in critical areas is essential for accommodating the full spectrum of exercises, preserving the suit's integrity, and promoting an uninhibited workout experience.

Beyond the exercise session, we recognize the importance of aftercare. The exercise suit must not be a source of inconvenience when it comes to cleanliness. To address this, a thoughtfully designed mechanism for washing and sterilizing the suit is important. This mechanism should not only maintain hygiene standards but also preserve the longevity of the suit, ensuring that it remains a reliable companion for the user's fitness journey.

3.3 Architecture of our suit

Our suit's design architecture can be broken down into 3 parts:

- Sensor
- Micro-controller
- Connectivity

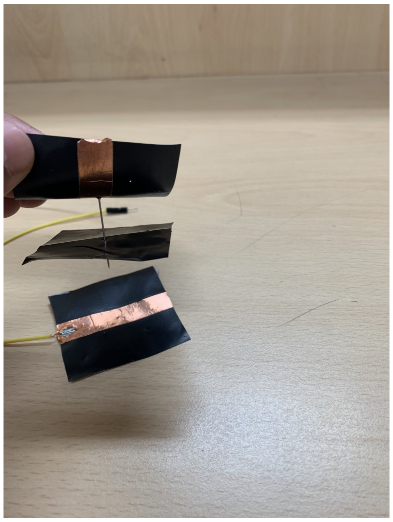

((a)) Dissected view of the 3 layers of the sensor

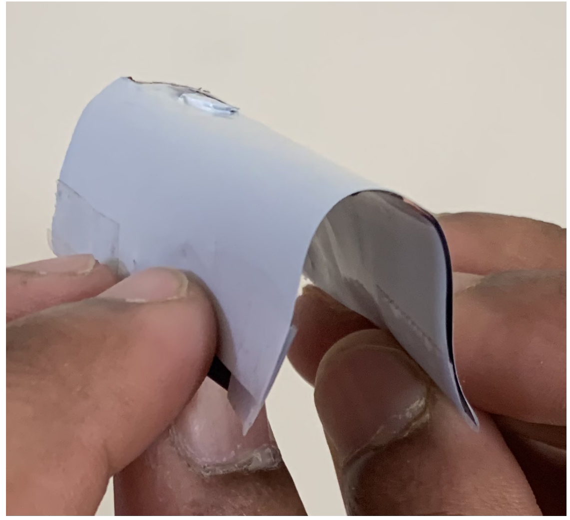

((b)) The sensor in bent position

Figure 3.1: Pictures of a single sensor

3.3.1 Sensor

A sensor is a device that translates any physical measurement into a signal, in most cases into an electrical signal. We are using Piezoresistive pressure sensors that generate a signal as a function of the pressure applied on it.

Piezoresistivity is an electromechanical effect that is characterized by a change in electrical resistivity in a material with applied mechanical change. This change is commonly a reversible microstructural change, such as a change in the degree of electrical continuity in the material [13]. We will be discussing about the sensor in detail in the coming section.

We are using Piezoresistive pressure sensors, with velostat as the diaphragm. We are engineering our sensor using the crossbar architecture. It typically consists of three layers. 3.1(a) The top and bottom layer contain the electrodes, with a pressure sensing layer sandwiched in between the two. The top and bottom electrodes are orthogonal to each other in orientation, thus forming a mesh-like structure. The middle layer being a piezoresistive sensor, in our case velostat, will act as an insulator until an external pressure is applied. One of the layers, let's say the top layer will be set at a constant DC voltage while the other layer, the bottom layer, will be connected to a microcontroller which will read any voltage that is applied to the bottom layer. When an external pressure is applied on the sensor, the velostat's resistance will decrease and thus change the potential difference between the top and bottom layer.

Each sensor is a 4cm × 4cm pressure sensor matrix with three layers. The top layer and the bottom layer were plastic sheets with copper electrodes in a vertical and horizontal alignment respectively[31]. Copper tapes were selected as electrodes because they have high conductivity. The middle velostat layer has a thickness of 106 ±2 μm The plastic sheet thickness was found to be 169 ±1 μm each, hence the total thickness of the pressure sensor matrix was approximately 440 μm, making it highly flexible. 3.1(b) The copper electrodes of 1 cm width were stuck onto the top and bottom layer facing the diaphragm in between. Cables were soldered onto copper tapes and all the sides of the pressure sensor were sealed thoroughly.

This sensor is flexible and, when sealed properly, is completely washable. We are using the sensor to measure the flexion of each muscle group. The degree of contraction and expansion of the muscle group will be directly correlated to the change in resistance from the neutral position.

3.3.2 Micro-controller

The microcontroller serves as the intricate brain of our innovative system, orchestrating all the essential computations required for evaluating the correctness of the user's form during exercise. Our overarching objective is to provide users with a seamlessly wearable suit, ensuring a hassle-free experience in the gym. To accomplish this, a pivotal requirement emerges—the imperative need for the exercise suit to be wireless.

While it may be challenging to completely eliminate the wired connections between sensors and the microcontroller, we have strategically focused on enhancing the user experience by enabling wireless communication and a wireless power source. This strategic approach aims to alleviate any discomfort associated with wired connections, facilitating unrestricted movement and flexibility during workouts.

Delving into the specifics, our sensors, engineered with efficiency in mind, boast low power consumption, allowing them to be effortlessly powered by a compact battery pack. This not only contributes to the overall portability of the suit but also aligns with our vision of creating an exercise companion that requires minimal effort to wear.

The crux of our wireless design revolves around three key principles: wireless connectivity, low power consumption, and user-friendly functionality. In pursuit of these objectives, we have chosen to implement the ESP32 microcontroller. The ESP32 is a versatile microcontroller renowned for its dual support of both Wi-Fi and Bluetooth technologies, enabling seamless communication with the user's mobile phone

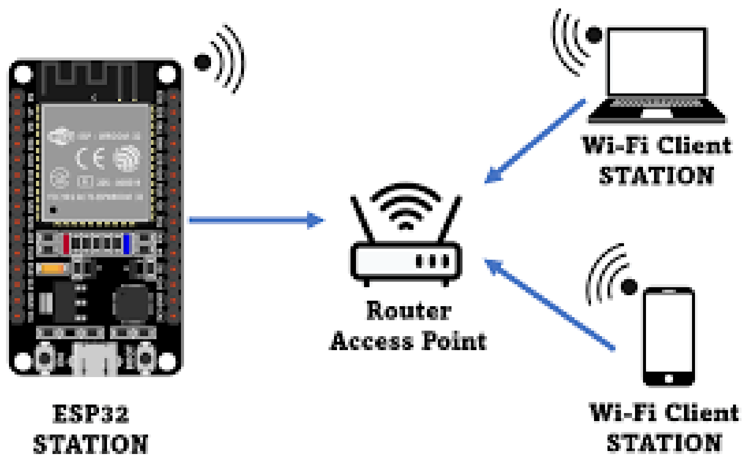

Figure 3.2: Connection of sensor to microcontroller

or other compatible devices. This ensures real-time feedback delivery, a crucial aspect for enhancing the effectiveness of the user's workout routine. 3.2

An additional advantage of the ESP32 lies in its low average power consumption during active mode, measuring at a mere 78.32 mW.[32] This renders the suit compatible with a wide range of regular battery packs, such as 6V or 9V, eliminating the need for bulky power sources. The lightweight nature of the ESP32 further contributes to the overall comfort of the suit, as it can be inconspicuously and securely integrated into the fabric of our innovative exercise ensemble.

In essence, our meticulous consideration of wireless functionality, low power requirements, and user-friendly design, coupled with the incorporation of the ESP32 microcontroller, epitomizes our commitment to creating an exercise suit that seamlessly integrates with the user's routine, promoting both comfort and effectiveness in their fitness journey.

3.3.3 Connectivity

In our research, the connectivity aspect plays a crucial role in enhancing the effectiveness and accuracy of our exercise suit. We have meticulously integrated 5 sensors in prototype 1 and expanded to 6 sensors in prototype 2, strategically placed to capture comprehensive data on muscle activity and movement patterns during exercise routines.

Our primary objective revolves around identifying and rectifying flaws in exercise form, with a specific focus on the flexion of the back. This deliberate choice stems from two pivotal factors. Firstly, the back constitutes one of the largest muscle groups in the human body, harboring significant implications

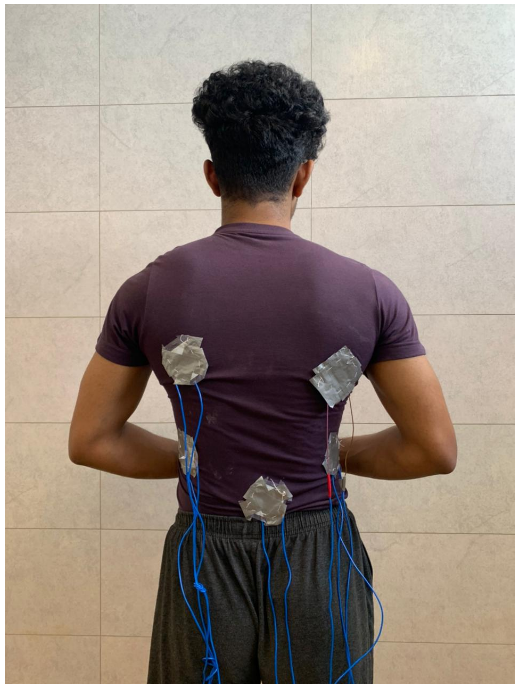

Figure 3.3: Placement of sensor for our prototype 1

for overall physical performance and health. Secondly, it shoulders the brunt of weight loads during compound exercises, rendering it particularly susceptible to injuries spanning from minor muscle pulls to severe spinal dislocations.

The strategic placement of sensors emerges as a critical consideration in our methodology. Our approach emphasizes positioning the sensors on muscle tissue that experiences the most pronounced stretches and contractions throughout the exercise repetition cycle. By conducting a meticulous differentiation of muscle fiber activity across various points of its stretched length, we gain invaluable insights into exercise form and technique.

The process of pinpointing the muscle group in the back that undergoes maximal stretching across exercise repetitions necessitates a systematic approach. To achieve this, our test subjects wear a white shirt adorned with a precisely marked black dot matrix in their most relaxed state. The evenly spaced dots serve as reference points for capturing images of the subject in both the fully contracted and fully stretched positions during exercise repetitions.[33]

Through meticulous analysis of these images, we identify the section of the dot matrix that exhibits the most significant flexion between the contracted and stretched positions. This meticulous approach allows us to pinpoint the 7 most stretched muscle groups across repetitions of deadlifts and squats, averaged for comprehensive insights. These muscle groups include the left and right latissimus dorsi muscle, left and right teres major muscle, left and right deltoid muscle, and the thoracolumbar fascia muscle, arranged in decreasing order of stretch magnitude.

Now that we have identified the points to attach sensors let's look at the connectivity of the sensor. To capture the flexion in the sensors, we employ a method involving the creation of a voltage divider. This is achieved by incorporating a bias resistor across the sensor, forming a bridge. The flexion-induced resistance change is measured by assessing the voltage drop across the sensor. Remarkably, our observations revealed a direct correlation between pressure and resistance, where the absence of pressure resulted in significantly high resistance and zero output voltage. Conversely, as pressure increased, the output voltage demonstrated a proportional rise. The mathematical representation of this relationship is encapsulated in the formula:

$$V_{out} = V_{in} * [R_b/(R_s + R_b)]$$

where V_{out} is the output voltage, V_{in} is the input voltage (which was fixed at 5 V), R_b is the bias resistor and R_s is the resistance of the sensor. 3.4

Now, transitioning to the broader system design, our approach involves embedding these sensors strategically onto a t-shirt, as previously detailed. The interconnected sensors are configured in the voltage bridge method, as elucidated above, ensuring a comprehensive and accurate measurement of flexion. This network of sensors is intricately linked to the ESP32, a powerful microcontroller, facilitating real-time monitoring and data processing. The ESP32 acts as the central hub, collecting data from the sensors and transmitting it wirelessly for further analysis. This wireless connectivity enables seamless communication with our dedicated device through WiFi, establishing a robust link between the wearable technology and our analytical framework. This holistic connectivity design not only enhances the efficiency of data collection but also enables a user-friendly and versatile system for in-depth analysis of exercise-related metrics.

3.4 Pressure Sensors

A sensor is a device that responds to a physical stimulus (such as heat, light, sound, pressure, magnetism, or a particular motion) and transmits a resulting impulse (for measurement or operating a control). For the pressure sensor, the physical stimulus is the pressure applied and a corresponding

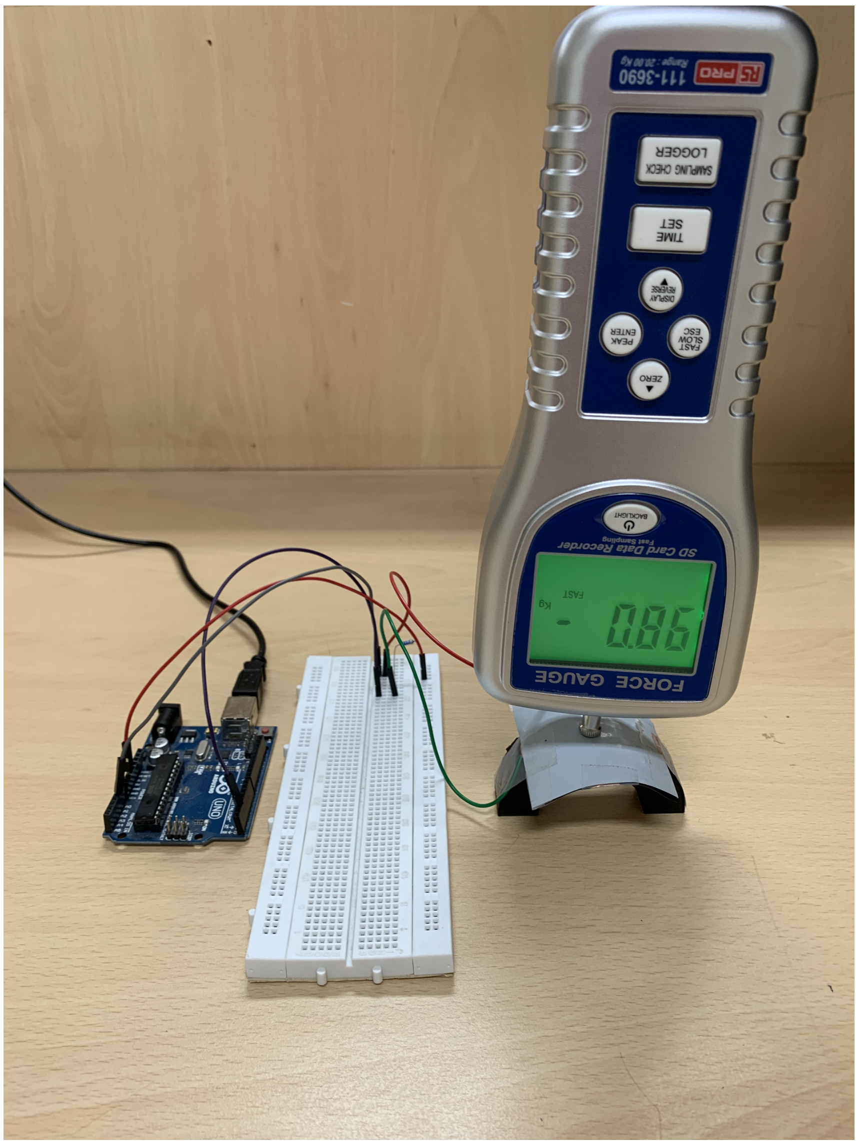

Figure 3.4: Connection of sensor to microcontroller

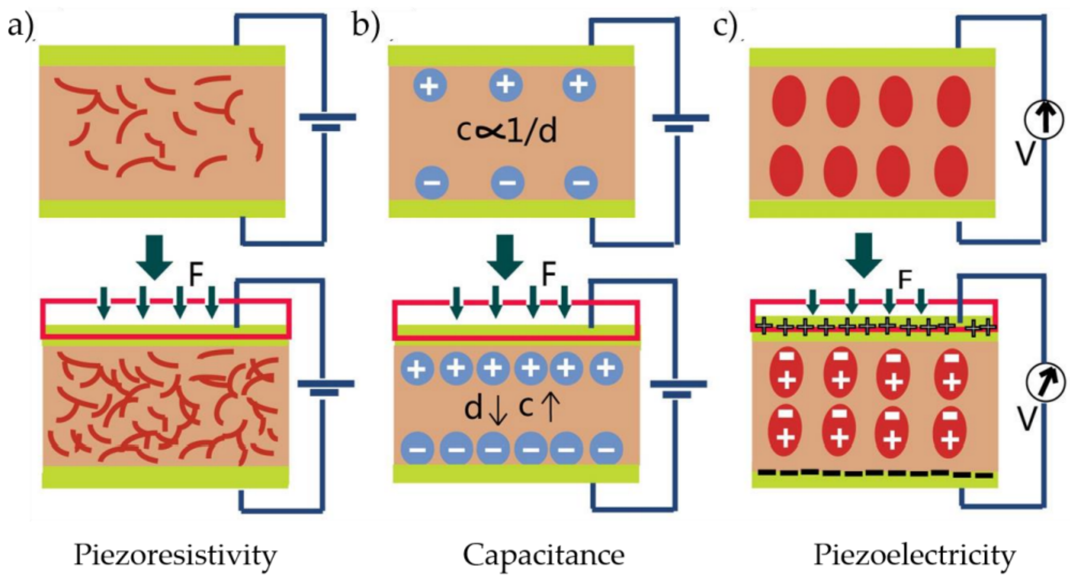

Figure 3.5: Schematic illustration of three common transduction mechanisms and representative devices: (a) piezoresistivity; (b) capacitance; and (c) piezoelectricity [40]

electric impulse is outputted. Generally, pressure sensors are of 3 types - piezoelectric [34], piezoresistive [12], or capacitive sensors [35, 36, 37, 38, 39].

Let us discuss these three types of pressure sensors in more detail.

- **Piezoelectric Sensors:** Piezoelectric sensors capitalize on the remarkable phenomenon of piezoelectricity, whereby they generate an electric charge in response to applied mechanical stress. The core of these sensors features a transduction element constructed from materials like lead zirconium titanate (PZT) ceramic or aluminum nitride (AlN) [41]. In the operational context, a typical configuration involves a sensing element that conveys fluid pressure to this transduction component. Critical to a well-designed piezoelectric pressure sensor is the maintenance of a constant diaphragm area. This design parameter ensures a direct proportionality between the force transferred to the transduction element and the applied pressure. Effectively, the force is then converted into a corresponding electric charge [42]. However, it's crucial to acknowledge that the use of piezoelectric sensors introduces a complexity—the need for a sophisticated electronic interface. The electronic interface complexity stems from the requirement of a charge amplifier. This component plays a pivotal role in converting the high-impedance charge output of the sensor into a more manageable and interpretable voltage signal [43]. Despite the intricate interface demands, piezoelectric sensors find application in various sectors, including medical devices (e.g., ultrasound transducers), industrial machinery, and pressure-sensitive consumer electronics.

- **Piezoresistive Sensors:** Piezoresistive sensors harness the electromechanical phenomenon of piezoresistivity, where the electrical resistivity of a material undergoes changes in response to applied mechanical stress. This effect involves a reversible microstructural transformation, affecting the material's electrical continuity. In the context of piezoresistive pressure sensors, the sensing material comprises a diaphragm positioned on a silicon substrate. This diaphragm flexes under applied pressure, causing a deformation in its crystal lattice. The strategically placed piezoresistors on the diaphragm experience alterations in their band structure due to this deformation, resulting in a discernible change in the resistivity of the material. For effective piezoresistivity, the material must exhibit electrical conductivity, leading to the prevalent use of metals and carbons. Composite materials, particularly polymer–matrix composites, dominate this arena due to their cost-effective fabrication [44]. Beyond the technical intricacies, piezoresistive sensors find diverse applications, playing vital roles in automotive systems, industrial machinery, and medical devices. The robust nature of piezoresistive sensors underscores their resilience in various operational environments. However, it's imperative to acknowledge their susceptibility to temperature variations, a consideration that necessitates careful integration in specific applications.

- **Capacitive Sensors:** Capacitive pressure sensors operate by gauging the alteration in electrical capacitance resulting from the movement of a diaphragm when pressure is applied. The fundamental principle involves a capacitor composed of two parallel conducting plates separated by a small distance. In this setup, one plate serves as the diaphragm, displaced under pressure, consequently modifying the capacitance within the circuit. These sensors offer versatility, capable of functioning across a broad temperature range, ensuring good repeatability in measurements. Moreover, their applicability spans a wide pressure spectrum, accommodating measurements from vacuum levels to high-pressure environments [31]. Capacitive sensors are categorized into normal, transition, touch, and saturation modes, providing adaptability to various operational contexts [45]. Despite their advantages, capacitive sensors exhibit non-linear output characteristics, necessitating sophisticated conditioning circuits and intricate computations for accurate interpretation. This non-linearity poses a notable challenge in certain applications, emphasizing the importance of careful consideration in sensor selection and system integration [46, 47].

Fig. 3.5 by Xu *et al.* summarizes the above accurately. Due to factors like simplicity, low cost, more durability, and a higher resolution output, piezoresistive sensors are chosen as the pressure-sensing material in this dissertation.

3.4.1 Velostat

Velostat stands as a noteworthy member of the force sensing resistor (FSR) category, falling within the realm of piezoresistive sensors. Operating as an analog sensor, the Force Sensing Resistor (FSR) exhibits a unique functionality wherein compression force induces a change in resistance. When force is applied to the FSR, its resistance decreases due to the conductive polymer it is constructed from. Under pressure, conductive particles within the polymer make contact, increasing the current flow through the sensor [48]. Yuan *et al.* provide detailed insights into Velostat through Scanning Electron Microscope (SEM) images at 5000x magnification. These Fig. 3.6, vividly depict the physical alterations Velostat undergoes under stress. Carbon particles are represented by white spots, while the black spots signify gaps in polymer clusters. Notably, the average gap between polymer clusters reduces from 1μm to 0.6μm when external pressure is applied [49]. Velostat has found widespread application in diverse research scenarios, including finger gesture recognition [50], smart chairs [51] , footprint pressure system [52], in-socket pressure sensing [53], wearable sensors [54], real-time tracking system [55], etc. Its popularity stems from its cost-effectiveness compared to other piezoresistive materials like graphene-based polymeric composites, porous graphene, and carbonized melamine, which pose fabrication challenges [56]. A comprehensive study by Del Prete *et al.* delves into the metrological properties of Velostat, reporting commendable performances in response function, calibration, repeatability, sensitivity, time drift, hysteresis, and dynamic response. This substantiates Velostat's efficacy as a pressure sensing material and its suitability for a range of applications, combining affordability with reliable performance [57].

3.4.2 Related Works

Several implementations of the sensor design mentioned above have been reported in the literature. Sundholm *et al.* present a flexible pressure sensing mat with a sensing area of 80 cm $\times$ 80 cm that is used to detect gym exercises [58]. They used 80 electrodes with a pitch of 1cm for each of the two layers with a conductive textile as a sensing element. From the pressure readings collected by this mat, they were able to classify between 10 different gym exercises with an accuracy of just less than 90%. Suprapto *et al.* created a 16×16 sensor matrix in the crossbar architecture for foot pressure measurements

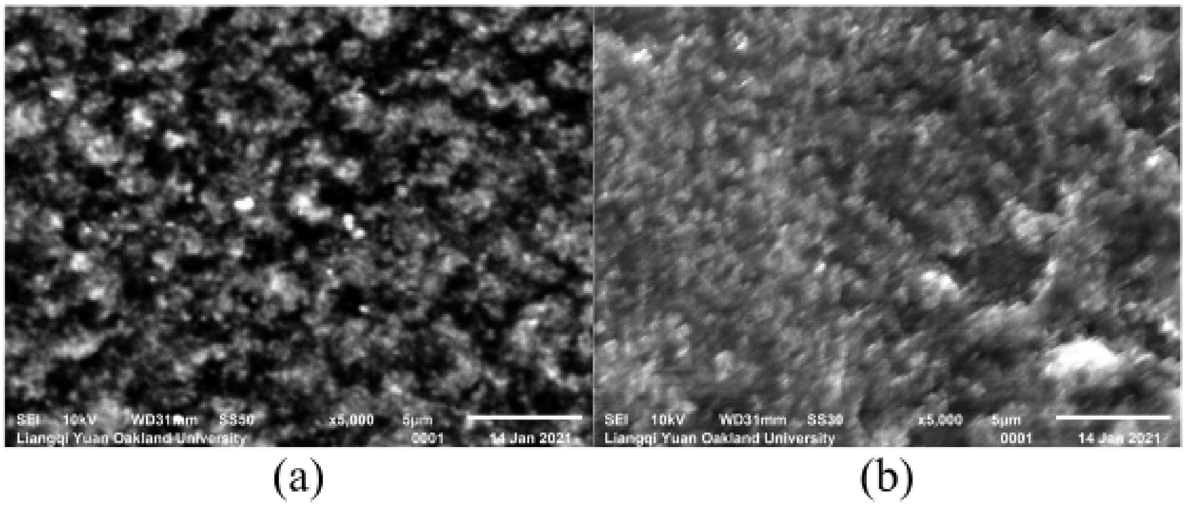

Figure 3.6: SEM image of Velostat material at 5000 times magnification, (a) without pressure and (b) with pressure. [49]

[48]. They used velostat as the piezoresistive material. The sensor matrix they developed was compared against the gold standard of human plantar pressure detection and reported satisfactory results. Gala *et al.* developed a system that can detect user presence in a chair using velostat-based pressure sensors that send real-time pressure data to a website which can then be used to set customizable alerts. These sensors can not only detect the presence of a user but can provide details on the anatomical well-being of the user, like detecting scoliosis [59]. Yuan *et al.* developed a 27×27 velostat-based pressure sensing array that can be used for object recognition. From the pressure images collected from the mat, they used the neural network ResNet-PI to classify 10 objects and reported an accuracy of 0.9854 for the same [49]. Our lab group has done several projects on the same. In [56, 60, 61] a 4×4 low-cost, flexible pressure sensing matrix was developed for activity monitoring and tracking recovery in stroke patients. Anis *et al.* further tested the mechanical reliability of these velostat-based sensors in [62]. They report an observed deviation in output voltage was 0.95% for 15 mm, 0.95% for 20 mm, 0.97% for 25 mm, and 2.2% for 30 mm bending radii, for 150 bending cycles, with respect to the flat position. They also proposed a two-parameter calibration model which can be used to minimize these deviations further. Mohee *et al.* [63] developed a flexible writing pad. The writing area is 5 cm × 5 cm with an effective pixel area of 0.06 mm^2

Chapter 4

Method and experimentation

4.1 Introduction

In this section, we will be dwelling on the details of experiments we have done to confirm the practicality and accuracy of the suit. We are testing on the basis of accuracy, usability, and feasibility. We will be discussing 2 experiments done. The first experiment was done with prototype 1, which has 5 sensors - The left latissimus dorsi muscle, Right latissimus dorsi muscle, Left teres major muscle, Right teres major muscle, and the thoracolumbar fascia muscle. The experiment was done only on deadlifts. The second experiment was done with prototype 2, which has 6 sensors - Left latissimus dorsi muscle, Right latissimus dorsi muscle, Left teres major muscle, Right teres major muscle, Left deltoid muscle, and Right Deltoid muscle. The experiment was done only for 3 exercises - “deadlift”, “squat” and “rows” - and was tested on 3 people.

4.2 EXPERIMENT 1

Let’s look at the exercise we are analyzing for this experiment. The deadlift, an essential compound exercise within the realm of weight training, serves as a powerhouse for targeting various muscle groups, predominantly focusing on the lower back and legs.[64] The intricacies of this exercise delve into the engagement of specific muscles such as the lower latissimus dorsi, hamstrings, glutes, hips, knees, ankles, and the core. Its execution involves lifting a barbell from the floor to mid-thigh height, achieved by extending the ankles, knees, and hips while maintaining a neutral to slightly extended spine, complemented by fully extended elbows[65]. Below Diagram 4.1 shows the step-by-step movement of the Deadlift from start to finish.

Figure 4.1: Step-by-Step Motion of Deadlift

Despite its effectiveness in muscle engagement, the deadlift stands out as one of the exercises notorious for its potential to induce injuries. Various studies have underscored the prevalence of injuries associated with the deadlift, affecting muscle groups like the pectoralis major, hamstrings, anterior superior iliac spine, lumbosacral region, and the knee meniscus. These injuries, stemming from improper form or posture, are not exclusive to beginners; even seasoned experts face the risk of such complications.[7, 8, 9, 10]

A comprehensive exploration of the risks associated with the deadlift is explained by the study conducted on 104 expert powerlifters. The findings revealed that a significant 31% of injuries occurred during deadlift training sessions. This statistic underscores the universal vulnerability to injuries during the execution of the deadlift, transcending skill levels and expertise.[11]

The intricacies of maintaining proper form during the deadlift cannot be overstated, and researchers have consistently emphasized the role of torso positioning in injury prevention. Notably, a more upright torso has been proven to be instrumental in reducing the risk of injuries associated with the deadlift. This underscores the importance of not only engaging in this powerful exercise but doing so with meticulous attention to form and technique, particularly regarding the alignment of the torso.

4.2.1 Data collection

Data was collected from an expert subject with experience in weightlifting (with consent and following the Institute's policy). The participant engaged in a series of 20 repetitions of deadlifts, skillfully executing both correct and incorrect forms. Notably, to mitigate any potential risk of injuries, the repetitions

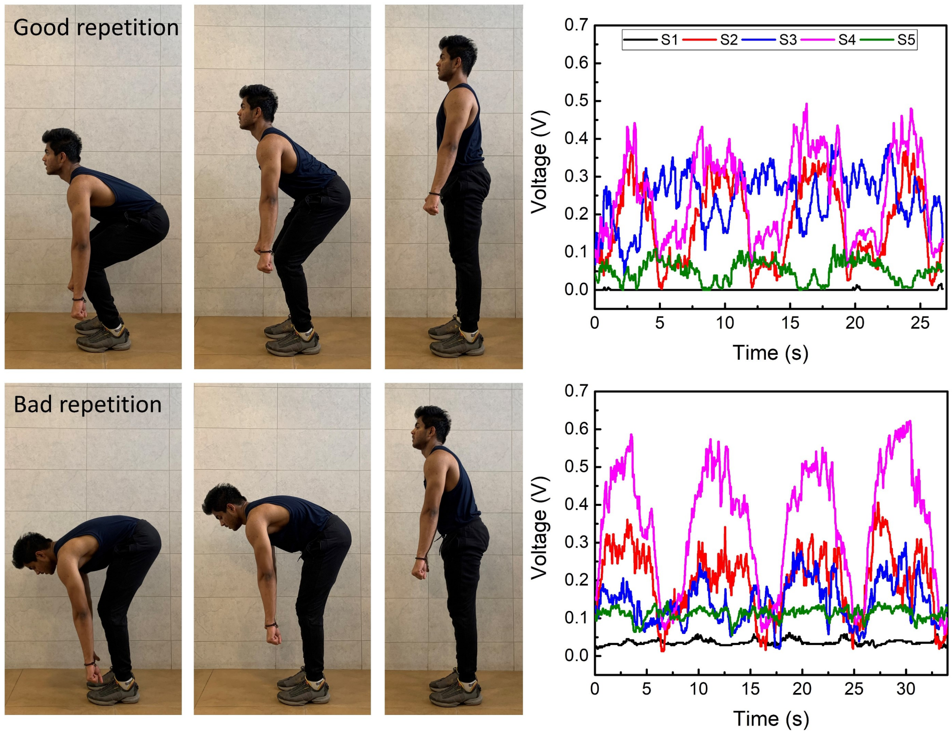

Figure 4.2: The difference between good and bad physical form for a repetition of deadlift along with the corresponding sensor outputs for four reps.

were performed without any external weights. This precautionary measure aimed at safeguarding the participant's well-being allowed for a focused examination of the exercise suit's connectivity without compromising safety. The sampling rate of the sensor is 50Hz and 20 repetitions were done with each repetition taking about 6-10 seconds. So we have about 8000 data points (400 data points for each repetition) for good posture and bad posture each.

The ensuing analysis delved into this raw data extracted from sensors during both instances of good and bad repetitions. The mean peak values were meticulously calculated, revealing a discernible contrast between the sensor readings associated with proficiently executed reps and those marked by improper form. 4.2 To enhance the interpretability of the gathered data, a thorough processing methodology was applied to distill essential patterns. This transformative step facilitated the classification of each repetition into two distinct categories: good or bad.

4.2.2 Data analysis

The initial phase of data analysis/processing involved a meticulous effort to extract meaningful information while mitigating the impact of external noise. This crucial undertaking was accomplished through the strategic application of a moving average filter (MAF).

The moving average filter operates by smoothing out fluctuations in data over a specified window of observations. At its core, the moving average filter aids in noise reduction and trend identification within time-series data. By computing the average of adjacent data points within a sliding window, abrupt spikes or erratic variations in the dataset are attenuated, revealing underlying patterns and trends with greater clarity.[66, 67, 68] This proves especially crucial in scenarios where the inherent noise in the data obscures meaningful information. Moreover, the moving average filter is instrumental in mitigating the impact of outliers, anomalies, or irregularities that may distort the true nature of the data. It provides a means of emphasizing the underlying trends while dampening the influence of transient fluctuations, contributing to a more accurate and robust representation of the dataset.

The next step is to decide the width of the MAF. Selecting the appropriate width for a moving average filter is a critical aspect of optimizing its performance in data smoothing and trend identification.[69] The width of the filter, often referred to as the window size or span, dictates the number of adjacent data points considered in the averaging process. The choice of this parameter is essential as it significantly influences the filter's ability to capture relevant trends while filtering out noise and fluctuations.

One primary consideration in determining the width of the moving average filter is the inherent trade-off between sensitivity and smoothness. A narrower window, representing a smaller span, renders the filter more responsive to short-term fluctuations but may result in a less smooth representation of long-term trends. On the other hand, a wider window, encompassing more data points, promotes a smoother output but may compromise the filter's ability to adapt to rapid changes in the data.[70] The method we are using to determine the appropriate filter width is the ”sum of absolute differences” (SAD) technique. This approach provides a quantitative measure to assess the performance of the filter across different window sizes.

To implement the SAD method, the process begins by applying the moving average filter to the dataset under consideration with a range of window sizes. For each window size, the absolute differences between the filtered values and the original data points are calculated and summed. The objective is to identify the window size that minimizes this cumulative sum of absolute differences.[71]

Essentially, the SAD method enables a systematic comparison of how well the moving average filter aligns with the original data across various window sizes. A lower sum of absolute differences indicates a closer match between the filtered and original data, suggesting that the chosen window size is better.

The flattening of the graph occurred notably when the window width surpassed the threshold of 35. So an average filter with a width of 40 is chosen.

The next step of processing is thresholding. As seen in the diagram 4.2, the peak value for the data stream differs for a rep with a good posture versus a bad posture. Using the peak differences, we obtained a threshold value separating the bad rep from the good one for each sensor. In the context of classification, thresholding proves invaluable by effectively segregating data points into predefined groups. This binary categorization simplifies data interpretation and creates a clear decision boundary.[72, 73, 74] Now the critical task is to find the threshold value. This was done by taking the set of peak values for good and bad reps data. The mean of these values gave us the threshold of the particular sensor data stream. These thresholds were used as clippers. Clipper, in the context of thresholding, serves as a dynamic filter, selectively retaining or excluding data points. Data points below the threshold are effectively clipped or set to zero. On the other hand, data points exceeding the threshold retain their original values, preserving the intrinsic differences between the data and the threshold. By employing a value as clippers, the thresholding process not only simplifies data interpretation but also enhances the effectiveness of subsequent analyses or classifications by isolating the most relevant information.

After thresholding, the five sensor data streams were combined into a single stream using the weighted sum of the values. The weight coefficient of each sensor can be calculated using two methods.[75] Method A: Based on the difference between the mean good peak value and the mean bad peak value. What this infers is that a sensor with a higher difference between the mean good peak value and the mean bad peak value can separate the good and bad forms making classification easier. Therefore their weighted coefficient should be higher. So in the core, the weight coefficient is directly proportional to the difference between the mean good peak value and the mean bad peak value.

or Method B: Based on the accuracy of feedback from each sensor. Sensor with a higher accuracy of prediction from the threshold is given higher weight.

For this experiment, we have used the latter method. Weight coefficients for each sensor were found by going through the tagged data and finding the accuracy by taking the difference between the number of correct and incorrect classifications. For every correct classification, 1 was added to the weight, and

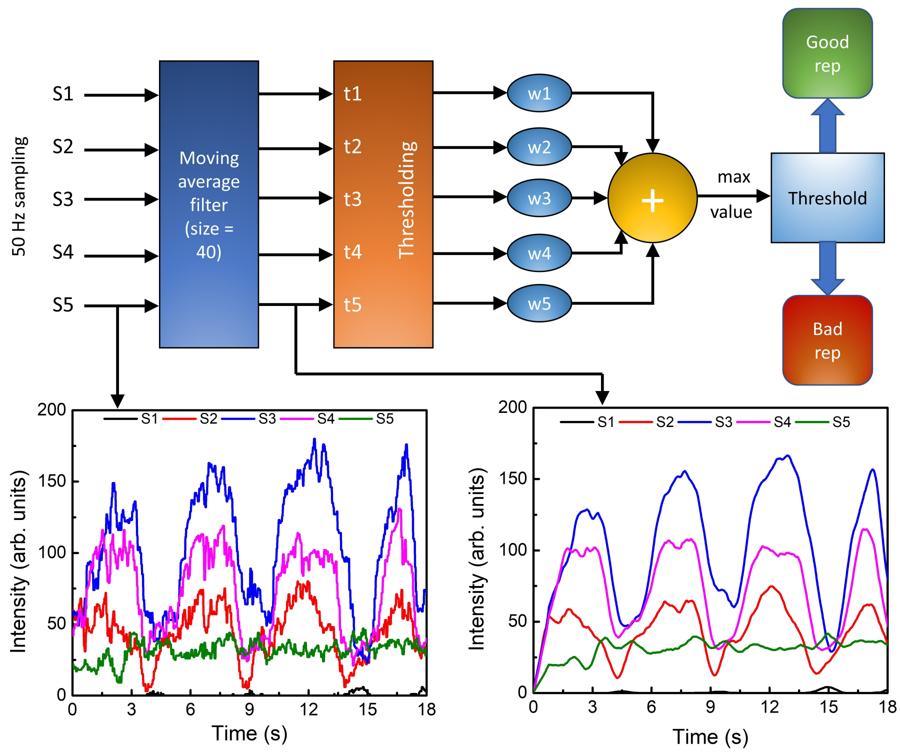

Figure 4.3: The data flow diagram for the algorithm used to classify the reps. The plots show the data stream for four reps after different stages

Table 4.1: Values for thresholds and weights for each sensor data stream

	Sensors				
	S1	***S2***	***S3***	***S4***	***S5***
Threshold	30.04	121.21	91.94	111.28	43.69
Weight ($\times 10^{-5}$)	58408	24116	24906	-8236	751

for each incorrect verdict, 1 was subtracted. The weights were then normalized such that $\sum W_i$ = 1. The maximum value of the weighted sum was then compared with a threshold to give the final classification.

The data flow diagram for the algorithm is shown in Figure 4.3, along with plots of the data stream at various points. The values for thresholds and weights for each sensor stream are given in Table 1 4.1. The threshold of the classification of the peak weighted sum was chosen based on the values of the two least weights because with these values, the bad rep classification happens only if at least two of the five sensors flag it as a bad rep. If the peak weighted sum was above this threshold, the rep was classified as a bad rep.

4.2.3 Results and discussion of experiment 1

The completion of the architectural framework, encompassing both software and hardware components, lays the groundwork for a comprehensive examination of the accuracy achieved by the developed exercise suit. Our evaluation focuses on Subject-1, who underwent a structured regimen consisting of 100 repetitions of deadlift exercises, comprising 50 good and bad reps. The sensor data derived from this exercise regimen was subjected to the classification model we devised. Remarkably, the classifier exhibited a noteworthy accuracy rate of 100% in identifying good repetitions, while achieving a commendable 90% accuracy in distinguishing suboptimal ones. As we delve into the assessment of the exercise suit's performance, a critical juncture emerges – the need for a solution that caters to a broad spectrum of users, holding both scientific and commercial significance.

While achieving pinpoint accuracy for an individual user is indeed commendable, there exists a need for prioritizing a more generalized approach in form and posture assessment. The inherent biomechanical variations among human bodies, influenced by factors such as body composition, flexibility, and muscle strength, brings out the necessity for a flexible and adaptable exercise suit. By adopting a generalized

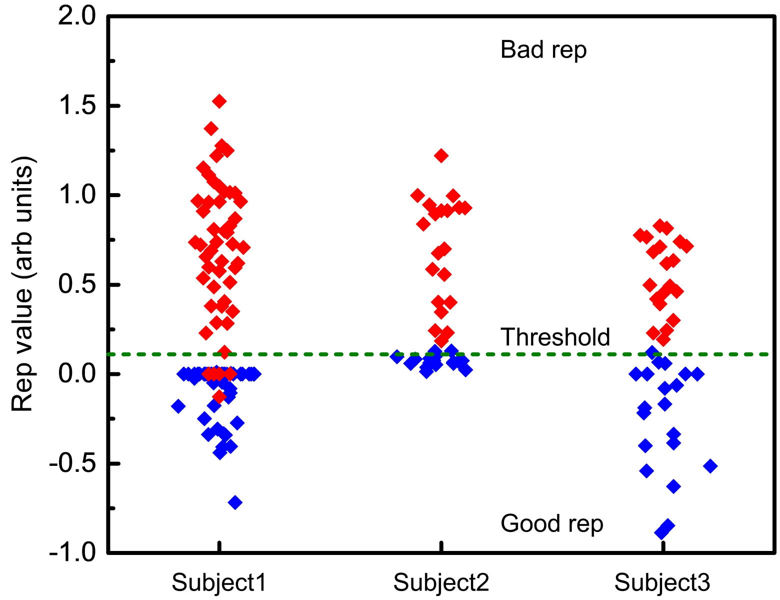

Figure 4.4: The peak weighted sum for each rep for three subjects. The blue dots and red dots represent the true value of the reps, while the threshold is used by the algorithm to classify the reps as good or bad.

approach, the technology becomes more inclusive, accommodating the diverse range of physiologies encountered within the user demographic. Such a generalized exercise suit has the potential to foster widespread health improvements by benefiting a larger population. Catering to diverse users ensures that the technology addresses a broader spectrum of fitness levels, making it a versatile tool for a larger audience. In line with this, our primary objective is to develop suits across various size ranges (XXS, XS, S, M, L, XL, XXL), promoting inclusivity over specificity. Beyond the health benefits, a more generalized approach proves economically advantageous. The scalability inherent in a generalized design facilitates economies of scale, rendering the technology more affordable and accessible to a wider audience. This strategic shift not only enhances the commercial viability of the technology but also ensures its availability to a larger demographic. To ascertain the robustness and adaptability of our developed model, we sought to evaluate its performance on other individuals. Subjects 2 and 3 were made to perform 40 repetitions of deadlift exercises, with 20 bad reps and 20 good reps. Utilizing the calibration results obtained from Subject 1, including thresholds and weight vectors, we applied the same parameters to analyze the data streams from Subjects B and C.

Encouragingly, the analysis revealed a noteworthy accuracy of 100% for both Subject 2 and Subject 3 in identifying bad posture, albeit with marginal variations in false positive rates (10% for Subject 2 and

5% for Subject 3). Fig. 4.4 visually depicts the experimental outcomes, highlighting the peak weighted sum threshold with dotted lines, and differentiating true values of good and bad repetitions through blue and red dots, respectively. Our comprehensive analysis yields an impressive overall classification accuracy of 95.5%, reinforcing the efficacy and versatility of the developed exercise suit across diverse individuals and reinforcing its potential as a valuable tool in the pursuit of optimal fitness.

4.3 EXPERIMENT 2

In this iteration of the experiment, notable modifications were made to the suit, as evident in the accompanying image 4.5. The adjustments primarily pertain to the repositioning of sensors, strategically placed on the Left and Right latissimus dorsi muscles, Left and Right teres major muscles, as well as the Left and Right deltoid muscles. This shift in sensor placement is an evolution from the insights gained in the white T-shirt with a dot matrix experiment discussed previously.

The pivotal motivation behind this adjustment was to extend the applicability of the sensor system beyond the confines of deadlift analysis. Drawing inspiration from the earlier experiment with the white T-shirt and dot matrix, our research aimed to investigate sensor positions conducive to classifying a spectrum of exercises, not limited to deadlifts alone. The experimentation involved a dynamic approach, with the test subject donning a T-shirt embedded with a black dot matrix and engaging in a diverse array of exercises.

The selection of exercises was deliberate, focusing on those where the posture of the back plays a critical role. The chosen exercises included deadlifts, squats, barbell rows, shrugs, and T-Bar pulls. Each of these exercises demands precise postural control of the back muscles during execution. To pinpoint the optimal sensor placement for capturing these nuances, our investigation honed in on the muscle groups displaying the most significant flexion between the contracted and stretched positions.

The six identified muscle points—Left and Right latissimus dorsi muscles, Left and Right teres major muscles, and Left and Right deltoid muscles—emerged as the focal areas experiencing the most pronounced flexion. Consequently, these specific positions were earmarked for sensor attachment, forming the basis for our experiment's sensor placement strategy.

For a more comprehensive analysis, a novel approach will be adopted for this experimental phase, building upon the insights gained from the initial experiment. The calculation employed in the first experiment primarily focused on variations in peak values. However, this experiment will broaden its

Figure 4.5: The suit design and position of the sensors.

scope to encompass two critical indicators: the disparity in peak values and the rate of change of these values. The inclusion of the rate of change as a secondary indicator is significant. An examination of sensor readings during the execution of the deadlift exercise reveals distinctive patterns between good and bad repetitions. 4.2 For the latter, observable sharp spikes in the sensor data denote a remarkably high rate of change. We will be able to incorporate this behavior/ pattern when considering the rate of change and its integration into our classification methodology. By incorporating the rate of change as an additional metric, the potential benefits extend beyond an increase in accuracy. Notably, this calculation proves invaluable in scenarios where the disparity in peak values alone might not suffice for a precise classification. The utilization of the rate of change serves as a nuanced and discriminating factor, allowing for a more refined categorization of exercises. Consequently, this multifaceted approach not only amplifies the precision of our classification but also underscores the versatility of the proposed methodology, especially in exercises with minimum variations in peak values. We will be looking at this method in detail in the following sections.

Now let's look at the 2 extra exercises we will be analyzing - Squats and rows.

A squat is a strength exercise in which the trainee lowers their hips from a standing position and then stands back up. During the descent, the hip and knee joints flex while the ankle joint dorsiflexes; conversely the hip and knee joints extend and the ankle joint plantarflexes when standing up. Squats

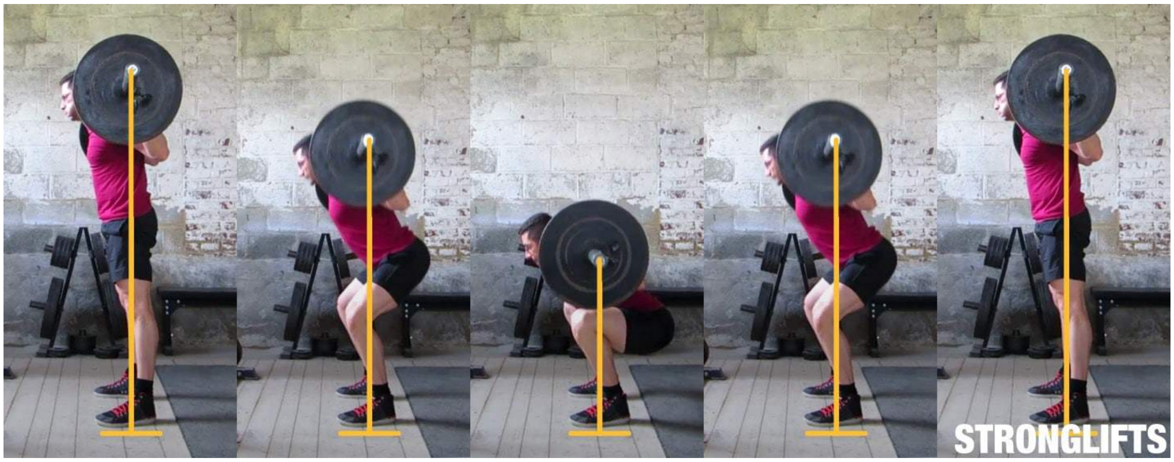

Figure 4.6: Step-by-step execution of a proper barbell squat

Figure 4.7: Step-by-step execution of a proper barbell row

also help the hip muscles. Squats are considered a vital exercise for increasing the strength and size of the lower body muscles as well as developing core strength. The primary agonist muscles used during the squat are the quadriceps femoris, the adductor magnus, and the gluteus maximus. The squat also isometrically uses the erector spine and the abdominal muscles, among others. Below Diagram 4.6 shows the step-by-step movement of a barbell from start to finish. [76, 77]

Barbell Bent Over Rows are a foundational compound exercise in strength training, concentrating on upper back development. To execute, one stands with feet shoulder-width apart, hinges at the hips to lean forward, and pulls the barbell towards the lower chest or upper abdomen, engaging muscles such as the latissimus dorsi, rhomboids, and trapezius. This movement also involves secondary muscles like the biceps and posterior deltoids, contributing to overall arm and upper back strength. The exercise promotes improved posture through targeted muscles responsible for scapular retraction. Diagram 4.7 shows the step-by-step movement of barbell rows from start to finish.[78, 79]

In both exercises, the form of the positioning and movement is critical to avoid injuries. In rows, practitioners are urged to exercise caution, emphasizing the maintenance of a neutral spine and proper form while steering clear of excessive swinging. It is imperative to avoid arching the back and ensure that it remains parallel to the ground throughout the entire motion, mitigating the risk of injuries associated with improper alignment. Similarly, squats demand a heightened awareness of form to safeguard against potential injuries. The emphasis here lies in bracing one's core effectively, with the back slightly caved in to maintain balance and a robust foundation. Deviating from this proper form by curving the back outward can place undue stress on the spine, leading to discomfort and a heightened risk of injuries. Despite the undeniable effectiveness of squats in engaging various muscle groups, the exercise is notorious for its potential to induce injuries when executed without due diligence to form and posture.

The pitfalls associated with squats are underscored by a plethora of studies, revealing the prevalence of injuries affecting muscle groups such as the pectoralis major, hamstrings, anterior superior iliac spine, lumbosacral region, and the knee meniscus. These injuries, often stemming from deviations in form, are not exclusive to beginners; even seasoned experts face the omnipresent risk of complications when executing squats improperly.[80]

A comprehensive exploration of the risks associated with powerlifting unveils a pertinent study conducted on 104 expert powerlifters. The findings revealed that a significant 42% of injuries occurred during squat training sessions among this cohort of seasoned individuals. This statistic underscores the universal vulnerability to injuries during the execution of the squat, transcending skill levels and expertise.

4.3.1 Data collection

The research data for this study was meticulously gathered from a cohort of three expert subjects, each possessing a profound background in weightlifting, all of whom participated willingly and in accordance with the protocols established by the Institute. Prior to the data collection process, explicit consent was obtained from each participant, ensuring their informed and voluntary participation. The participants engaged in a structured series of 20 repetitions of bad and good form each, of deadlifts, squats, and rows. It is crucial to underscore the participants' expertise, as they adeptly executed both correct and incorrect forms. An essential precautionary measure was implemented during the data collection phase to mitigate any potential risk of injuries to the participants. Notably, the repetitions were performed without the addition of external weights. While this may deviate from a conventional weightlifting scenario, this deliberate choice was made to prioritize the safety and well-being of the participants. By excluding external weights, the focus of the study shifted towards a meticulous examination of the connectivity and responsiveness of the exercise suit.

4.3.2 Data Analysis

In this section we will talk about the new analysis we are doing, why we are taking this extra step, and the improvement it causes.

As we have mentioned in the earlier section we are going to analyze the rate of change. Let's look at the Diagram 4.17 and 4.29. Here we can see that the peak value between the good and bad rep is not much different, so we will be compromising on the accuracy if we just do the classification based on the peak value. If we look closely at the figure what we notice straight away is that the shape is different, so if we are able to quantize the shape of the signal then we will be able to improve our accuracy. One method to classify these shapes is convolution, let's look at it in detail.

4.3.2.1 Convolution

Convolution is a fundamental operation in signal processing that plays a crucial role in analyzing and extracting information from various types of signals. What it does is that, it combines two functions to produce a third function, providing insights into the relationships between signals.[81, 82, 83] In the context of signal processing, convolution is used in tasks such as filtering, feature extraction, and most notably, shape classification. In signal processing domain, it is commonly employed to analyze how one signal modifies another[83]. The convolution operation is denoted by the symbol '*', and for two functions f(t) and g(t), their convolution h(t) is defined as:

$$h(t) = f(t) * g(t) = \int_{-\infty}^{\infty} f(\tau)g(t-\tau)d\tau$$

In discrete form, for two sequences f[n] and g[n], the convolution is represented as:

$$h[n] = f[n] * g[n] = \int_{k=-\infty}^{\infty} f[k]g(n-k)$$

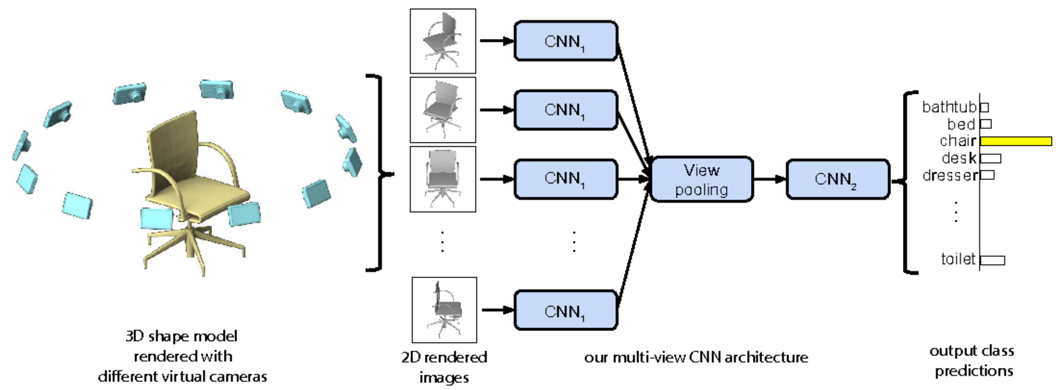

Figure 4.8: Numerous features are extracted from the image and are passed through CNN1 to extract view-based features. These are then pooled across views and passed through CNN2 to obtain a compact shape classifier.

4.3.2.2 Convolution in Shape Classification

Shape classification is a critical aspect of signal processing, particularly in fields such as computer vision and pattern recognition. Convolution is harnessed for shape classification commonly by convolutional neural networks (CNNs). CNNs are a type of deep learning architecture inspired by the human visual system, where convolutional layers play a pivotal role.

In shape classification, a group of signals, often represented as images, is input into a CNN for analysis. The convolutional layers of the network use convolution operations to detect and emphasize specific features within the signals, effectively learning hierarchical representations of the input data. As the signals pass through subsequent layers, more abstract and complex features are extracted.[84, 85]The convolutional layers utilize learnable filters or kernels, small-sized matrices that slide over the input signals to capture local patterns. These filters are responsible for identifying edges, textures, and other discriminative features that contribute to shape classification. The output of the convolutional layers is then fed into fully connected layers for final classification. Diagram 4.8 shows the step-by-step classification of images that happens in a CNN network.[86] In the Diagram, we can see multiple CNN neurons extracting features from the images. Then classification is done based on the extracted feature.

4.3.2.3 Advantages and Disadvantages of Convolution in Shape Classification

The advantages of using convolution are listed below [86, 87, 88]:

- **Local Feature Extraction:** Convolution enables the extraction of local features, allowing the network to focus on specific aspects of the signals. This is crucial for capturing intricate details in the shapes, contributing to accurate classification.
- **Translation Invariance:** The use of convolutional operations provides a degree of translation invariance. This means that the network can recognize shapes regardless of their position within the input signals, enhancing the robustness of the classification process.
- **Parameter Sharing:** Convolutional layers share parameters across the input signals, reducing the number of trainable parameters and improving the efficiency of the learning process.

The disadvantage of convolution is that the computation is very high when using it for shape classification. Our aim of doing the classification in the microcontroller will be hampered due to computational constraints. So we need to explore other methods of signal classification.

4.3.2.4 Analysis of rate of change of signal

Taking the derivative of a signal plays a significant role in shape classification, and its analogy to the second derivative of Taylor's series provides insights into the curvature and fine-grained details of the signal. Let's explore how this process aids in shape classification:

- **Rate of Change Information:** The first derivative of a signal measures its rate of change at each point. Peaks and troughs in the derivative correspond to significant changes in the original signal. In shape classification, distinctive features of a shape are often associated with points where the signal undergoes rapid changes. The first derivative identifies these crucial points in the signal.
- **Edge Detection:** Peaks and troughs in the first derivative can be indicative of edges or boundaries in the signal. By identifying edges through the first derivative, the shape classification algorithm can focus on critical regions, enhancing its ability to identify the shape of the signal.
- **Feature Extraction:** The derivative operation acts as a feature extraction mechanism. It transforms the signal into a new representation that emphasizes aspects relevant to the shape classification task. These extracted features can then be fed into a classification algorithm for more effective pattern recognition.

Analysis of the Rate of Change of the signal is a very feasible analysis. It can easily be done on our edge device. So let's walk through our analysis methodology.

4.3.3 Double Check Analysis Explained

We are aiming at a 2-step analysis. The problem with the analysis of experiment 1 is the following.

- If we are just looking at the peak value, it will be difficult to classify half reps. Half reps are the repetitions that didn't reach the extreme point of the movement. This is not exactly the wrong form. Half reps usually happen when doing a rep with a heavy weight.
- Just identifying bad reps with its peak value, will neglect some bad repetition. By avoiding the shape of the graph we neglect details of the movement and also other information like rep speed and tempo.

To rectify these limitation, we propose a refined two-step analysis that delves deeper into the sensor readings of each repetition. The initial check revolves around the peak value, acknowledging its importance while recognizing the need for a more nuanced approach. To reduce the false negatives, the peak value threshold is deliberately reduced in this first check.

The second check is introduced as a crucial step to provide a final verdict on the quality of each repetition, classifying them as either good or bad. This second check serves as a double-check mechanism, ensuring a more robust evaluation that incorporates the often-overlooked aspects of the exercise, such as the shape of the graph, rep speed, and tempo. By incorporating these additional parameters into our analysis, we aim to enhance the accuracy and feasibility of our classifier, offering a more comprehensive understanding of the nuances associated with different repetitions. Diagram 4.9 shows the overall flow of our analysis. In the diagram, the top section represents the first check- Peak value analysis, and the bottom section represents the second check - Rate of Change analysis. The result of both these steps will give our final verdict.

4.3.3.1 First check - peak value analysis

We passed our 6 sensor readings through a moving average filter. The moving average filter operates by smoothing out fluctuations in data over a specified window of observations. At its core, the moving average filter aids noise reduction and trend identification within time-series data. Diagram 4.10, 4.11, 4.12, 4.13, 4.14, 4.15 shows the sensor reading when the user does rows with a good form. The Diagram shows the readings before passing through a moving average filter. This reading is from one subject and each colour in the subplot represents each set done by the subject. Diagram

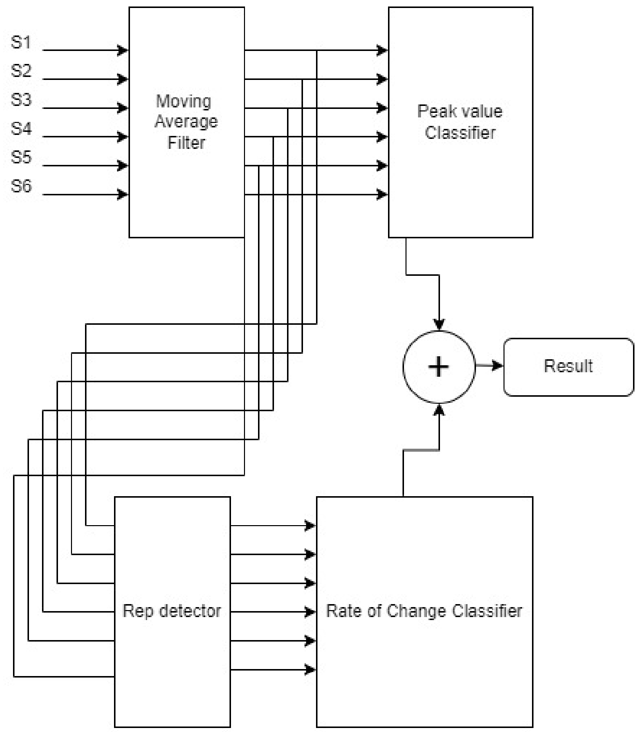

Figure 4.9: Block Diagram of the 2-step classification.

4.16, 4.17, 4.18, 4.19, 4.20, 4.21 shows the above sensor reading after passing through a moving average filter. Diagram 4.22, 4.23, 4.24, 4.25, 4.26, 4.27 shows the sensor reading when the user does rows with a bad form. The Diagram shows the readings before passing through a moving average filter. This reading is from one subject and each colour in the subplot represents each set done by the subject. Diagram 4.28, 4.29, 4.30, 4.31, 4.32, 4.33 shows the above sensor reading after passing through a moving average filter.

This step is exactly similar to the one done in experiment one. Further details about the moving average filter can be found in that section.

The next step is clipping of each sensor reading. We aim to find the threshold of each sensor to get individual verdicts from each sensor about the rep quality. In our last experiment, the threshold was found by just taking sets of peak values for good and bad reps data. The mean of these values gave us the threshold of the particular sensor data stream. This method can be optimised using the concept of gradient descent. Our goal is to enhance threshold accuracy by maximizing true positives and minimizing false positives. We perform a simple gradient descent on our threshold value with the loss function

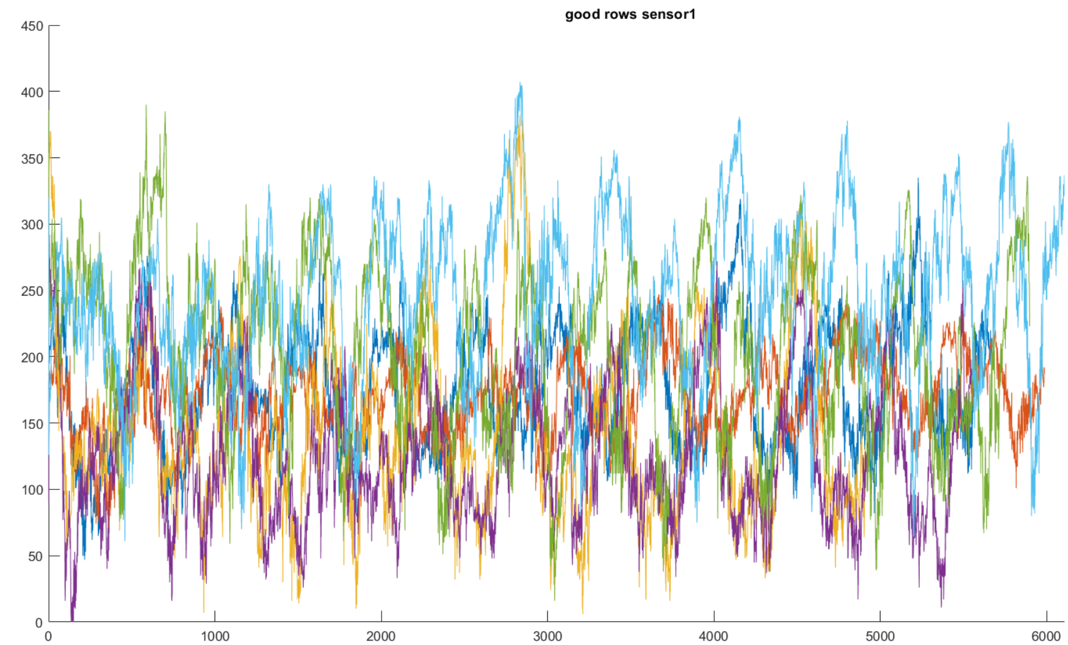

Figure 4.10: Readings from sensor 1 while doing rows with optimal form. Each colour represents different sets. The X-axis represents the timescale and the Y-axis represents the analog sensor readings.

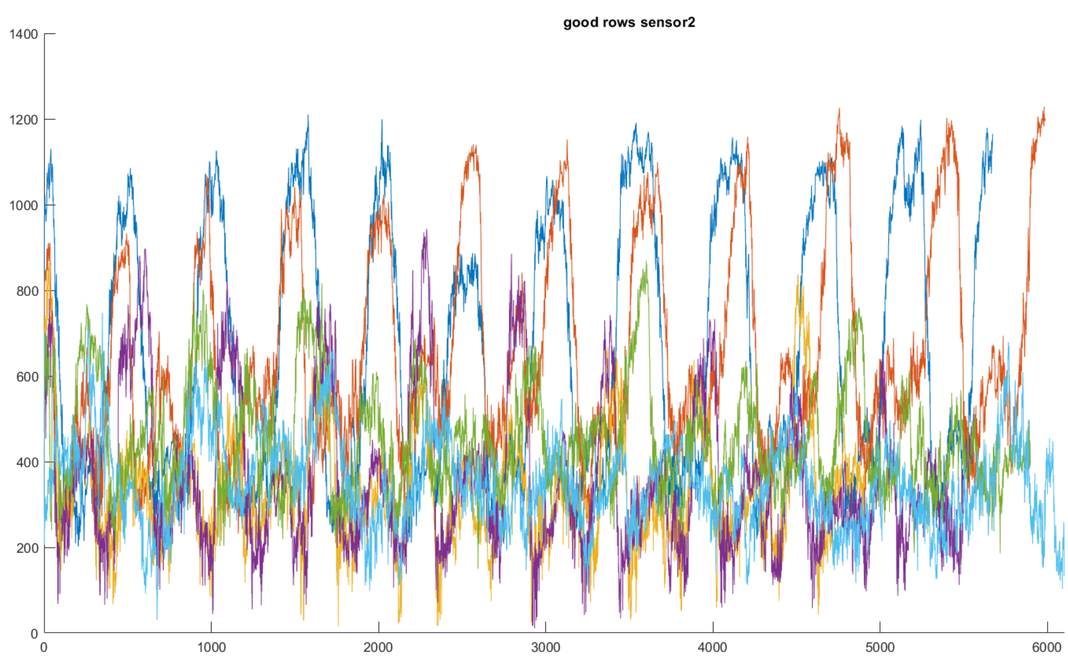

Figure 4.11: Readings from sensor 2 while doing rows with optimal form. Each colour represents different sets. The X-axis represents the timescale and the Y-axis represents the analog sensor readings.

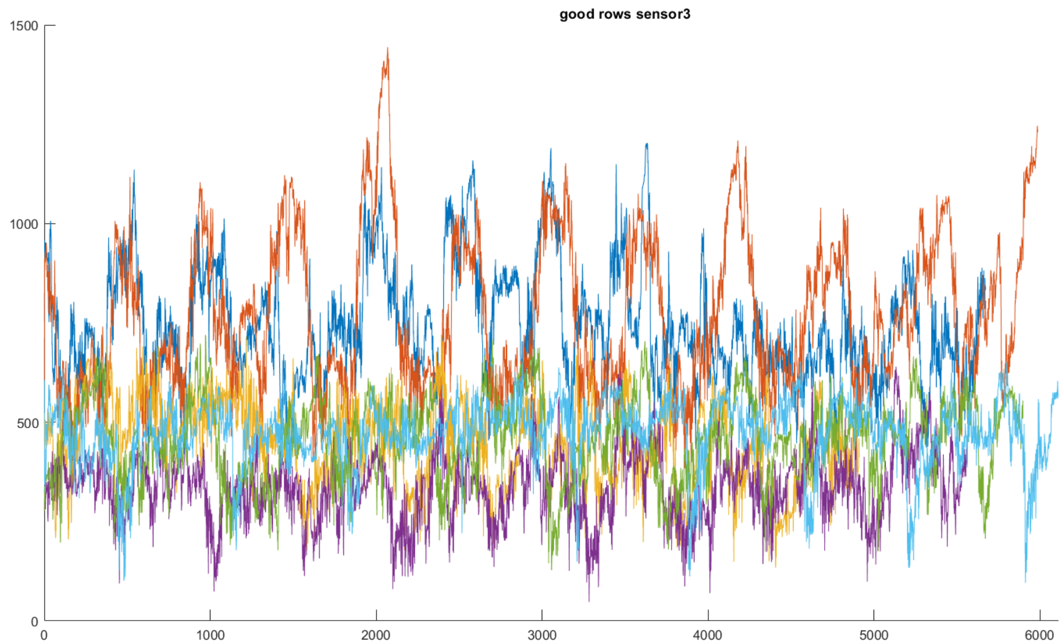

Figure 4.12: Readings from sensor 3 while doing rows with optimal form. Each colour represents different sets. The X-axis represents the timescale and the Y-axis represents the analog sensor readings.

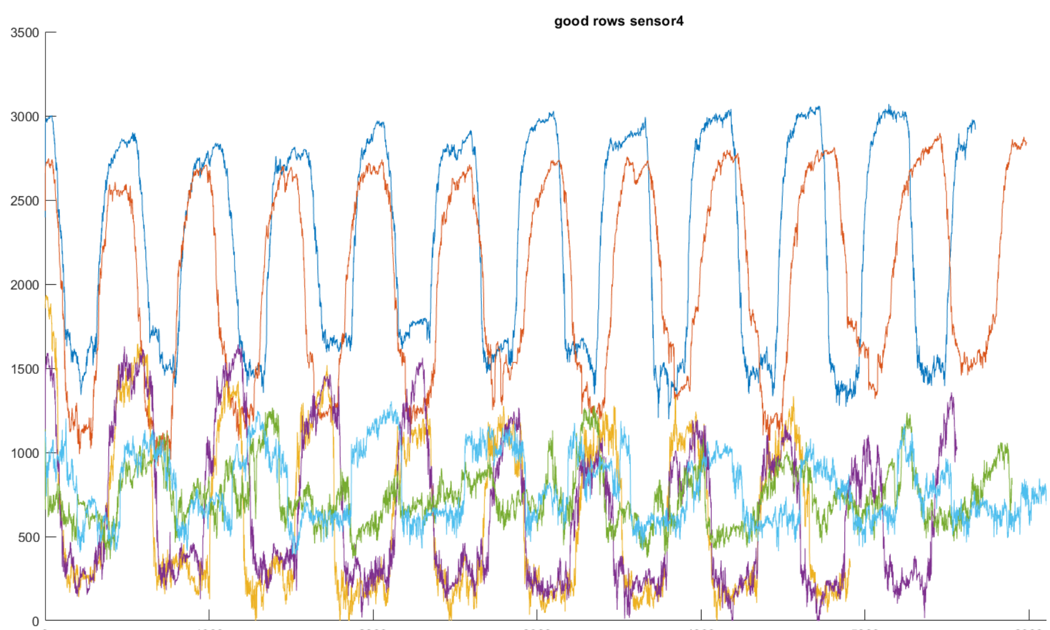

Figure 4.13: Readings from sensor 4 while doing rows with optimal form. Each colour represents different sets. The X-axis represents the timescale and the Y-axis represents the analog sensor readings.

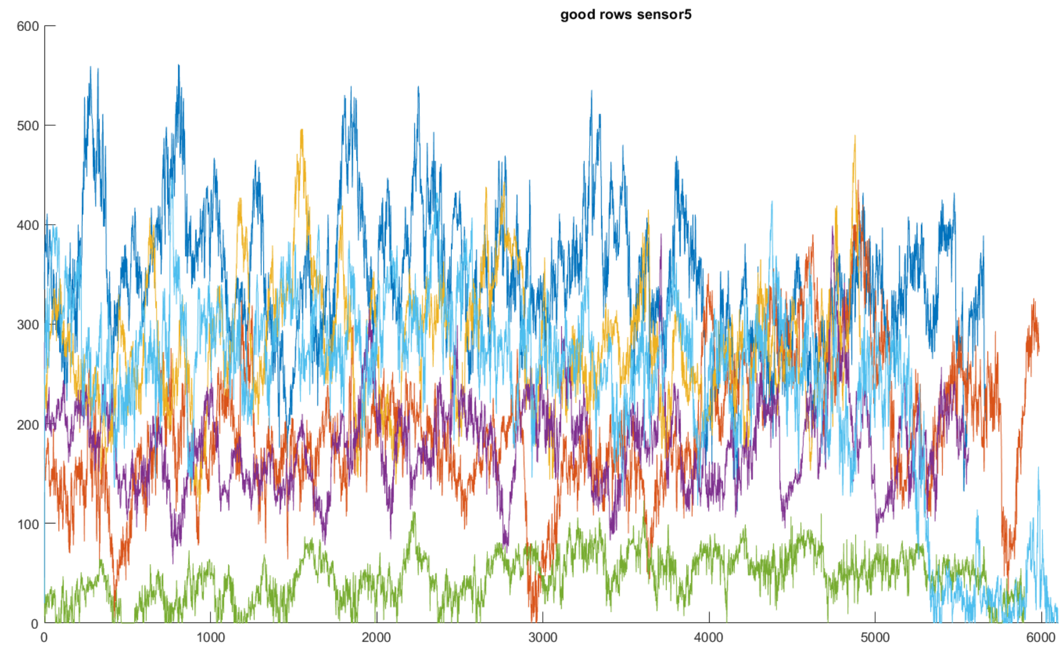

Figure 4.14: Readings from sensor 5 while doing rows with optimal form. Each colour represents different sets. The X-axis represents the timescale and the Y-axis represents the analog sensor readings.

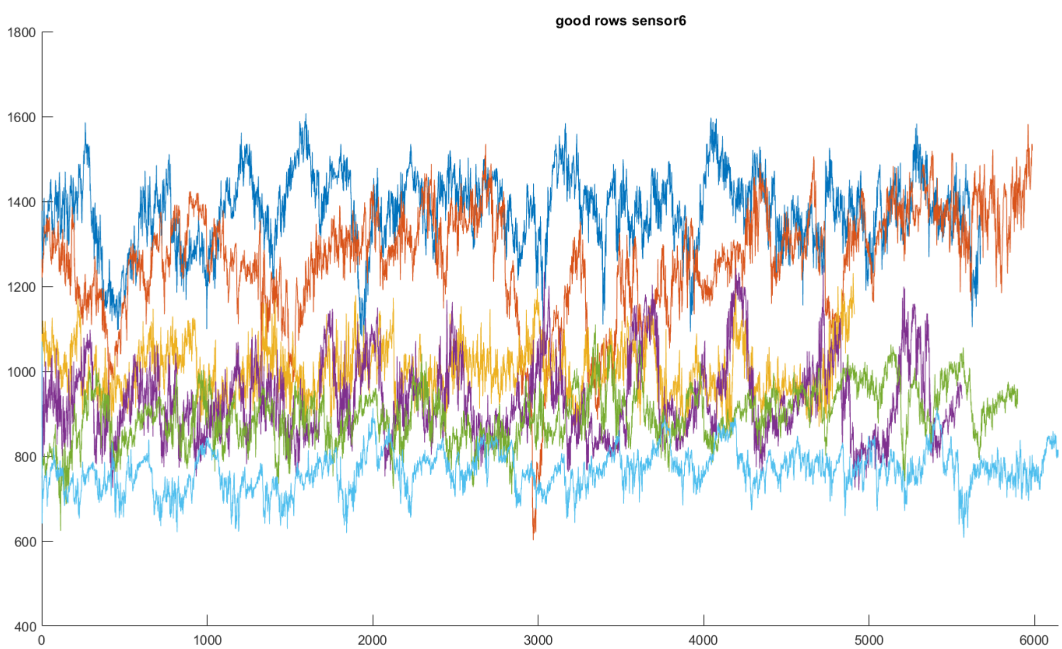

Figure 4.15: Readings from sensor 6 while doing rows with optimal form. Each colour represents different sets. The X-axis represents the timescale and the Y-axis represents the analog sensor readings.

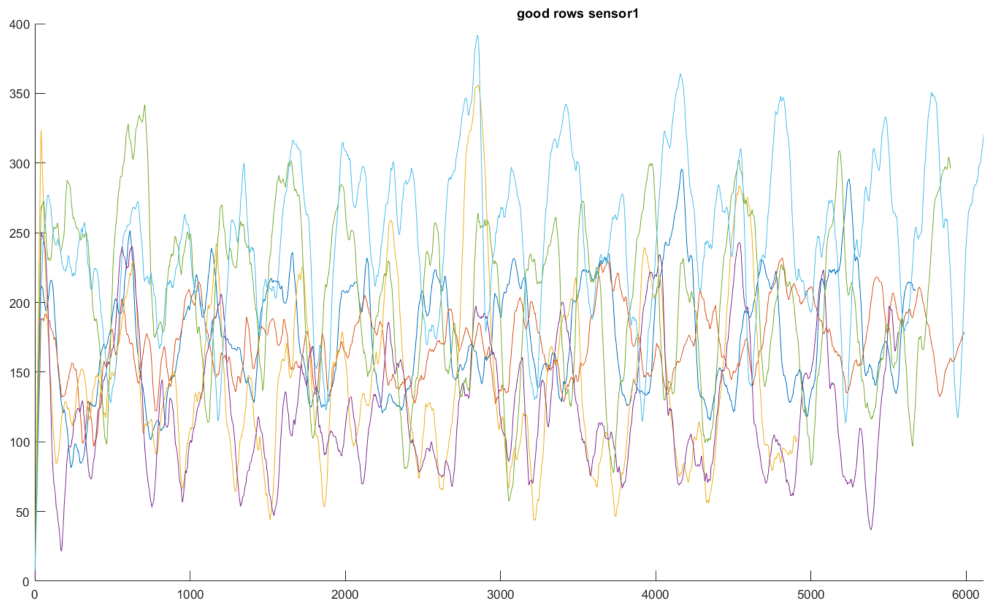

Figure 4.16: Readings from sensor 1 while doing rows with optimal form after passing through a moving average filter. Each colour represents different sets. The X-axis represents the timescale and the Y-axis represents the analog sensor readings.

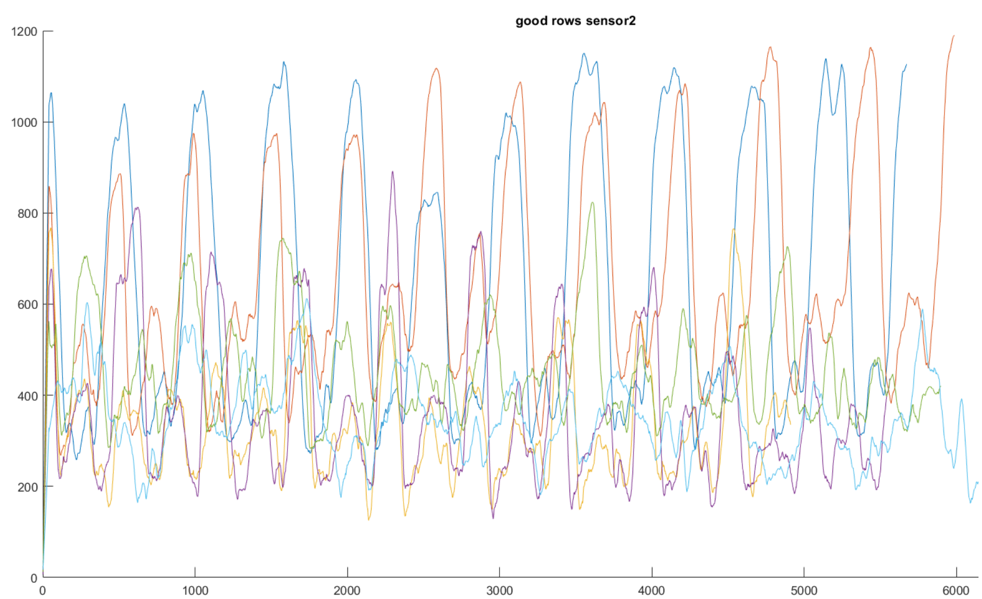

Figure 4.17: Readings from sensor 2 while doing rows with optimal form after passing through a moving average filter. Each colour represents different sets. The X-axis represents the timescale and the Y-axis represents the analog sensor readings.

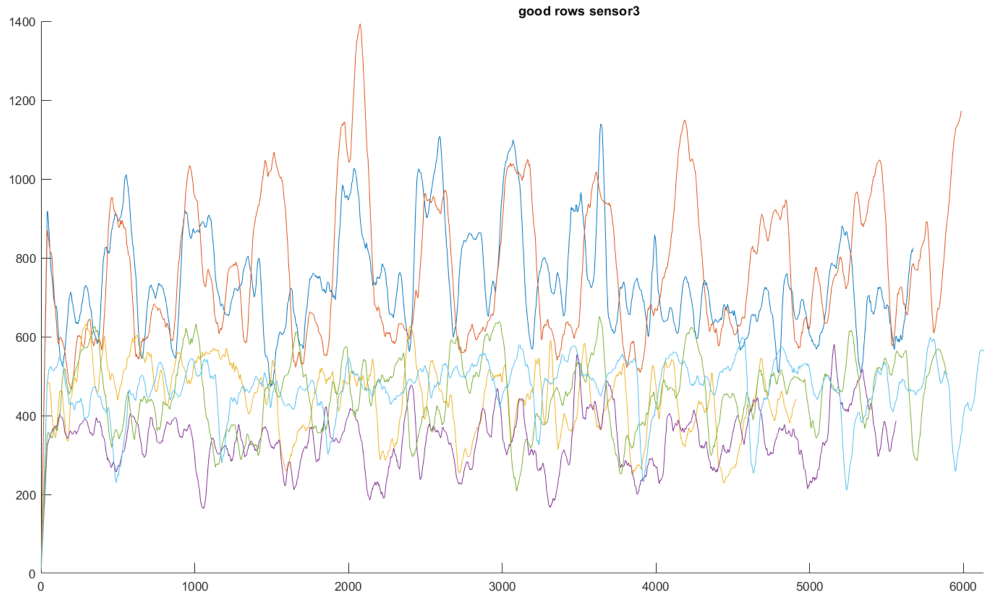

Figure 4.18: Readings from sensor 3 while doing rows with optimal form after passing through a moving average filter. Each colour represents different sets. The X-axis represents the timescale and the Y-axis represents the analog sensor readings.

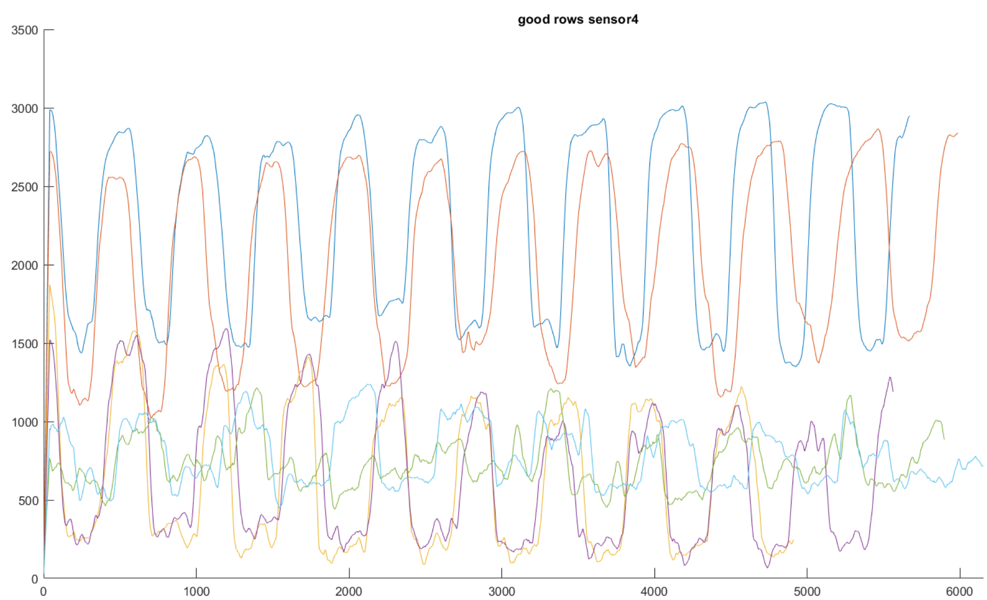

Figure 4.19: Readings from sensor 4 while doing rows with optimal form after passing through a moving average filter. Each colour represents different sets. The X-axis represents the timescale and the Y-axis represents the analog sensor readings.

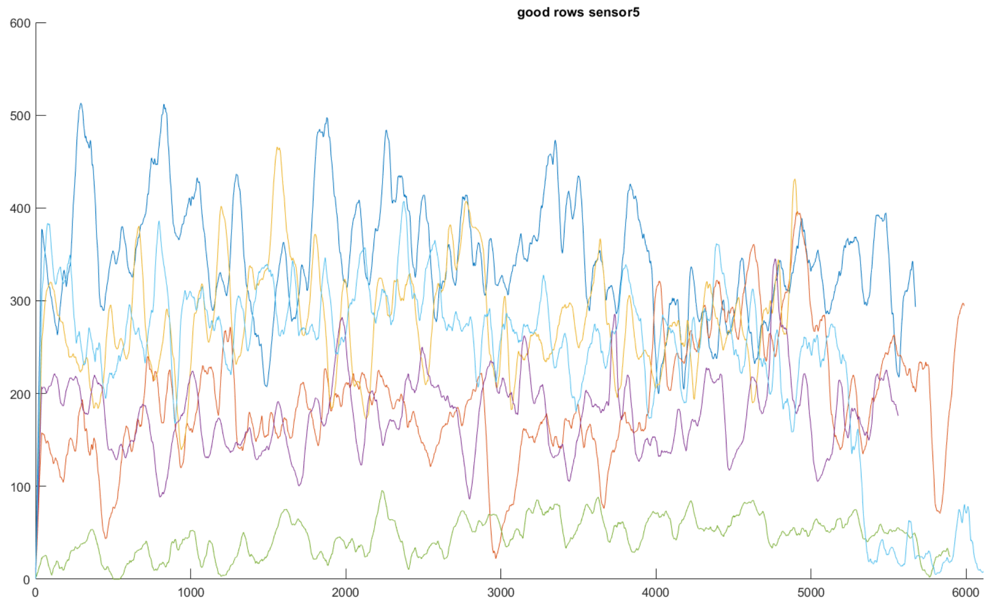

Figure 4.20: Readings from sensor 5 while doing rows with optimal form after passing through a moving average filter. Each colour represents different sets. The X-axis represents the timescale and the Y-axis represents the analog sensor readings.

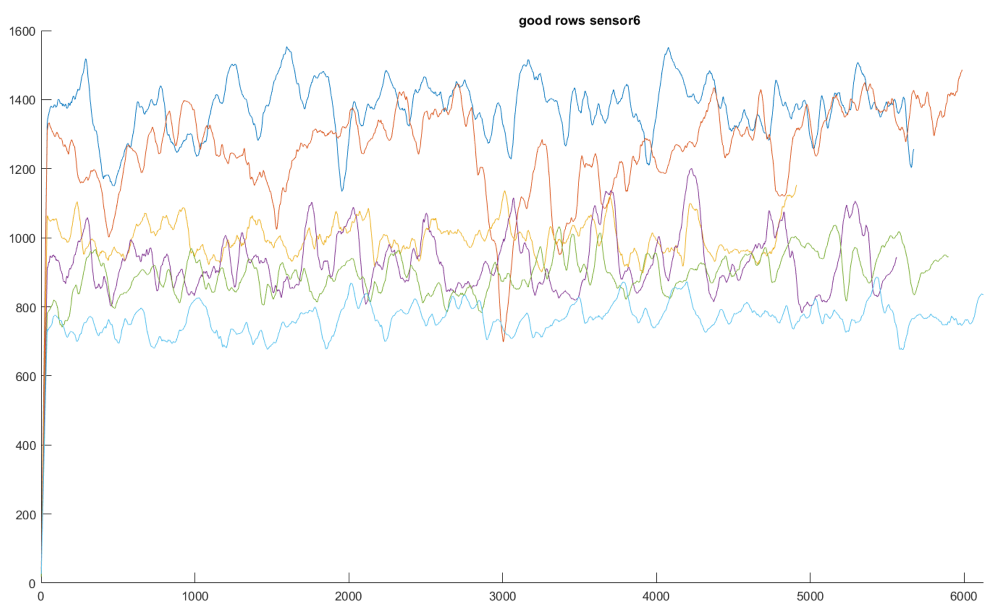

Figure 4.21: Readings from sensor 6 while doing rows with optimal form after passing through a moving average filter. Each colour represents different sets. The X-axis represents the timescale and the Y-axis represents the analog sensor readings.

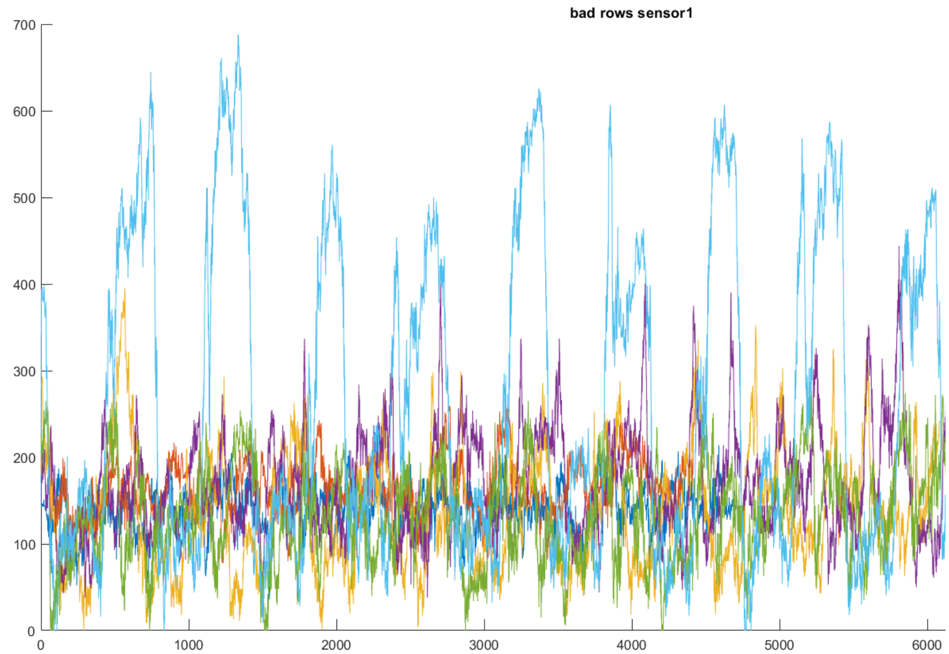

Figure 4.22: Readings from sensor 1 while doing rows with sub-optimal form. Each colour represents different sets. The X-axis represents the timescale and the Y-axis represents the analog sensor readings.

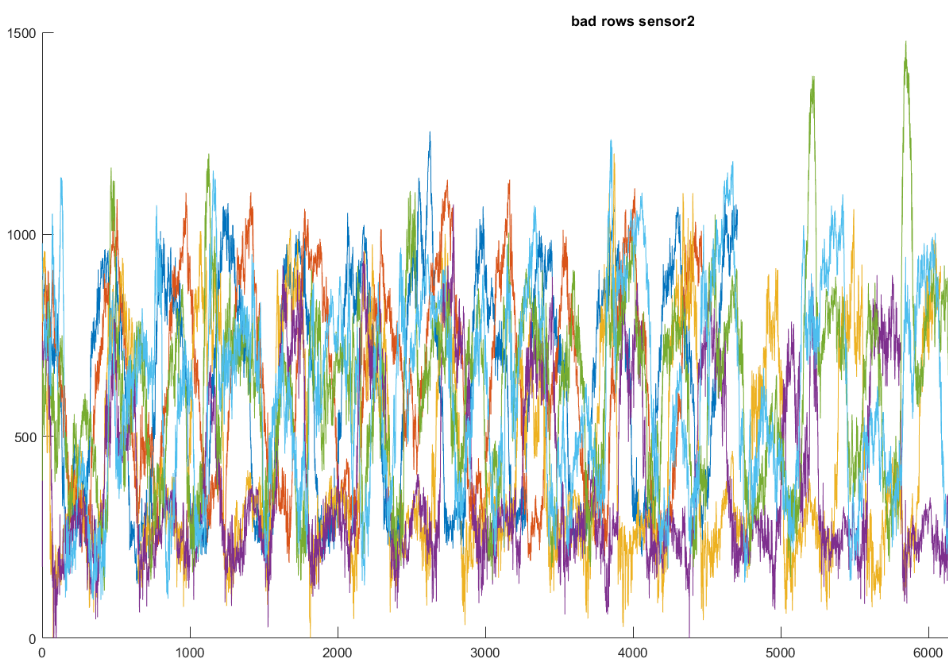

Figure 4.23: Readings from sensor 2 while doing rows with sub-optimal form. Each colour represents different sets. The X-axis represents the timescale and the Y-axis represents the analog sensor readings.

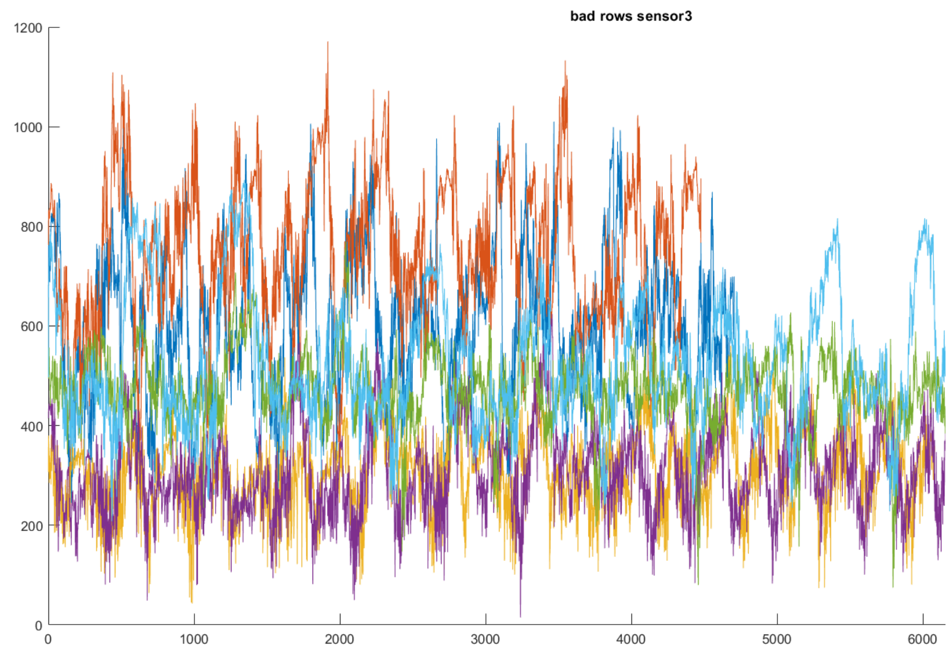

Figure 4.24: Readings from sensor 3 while doing rows with sub-optimal form. Each colour represents different sets. The X-axis represents the timescale and the Y-axis represents the analog sensor readings.

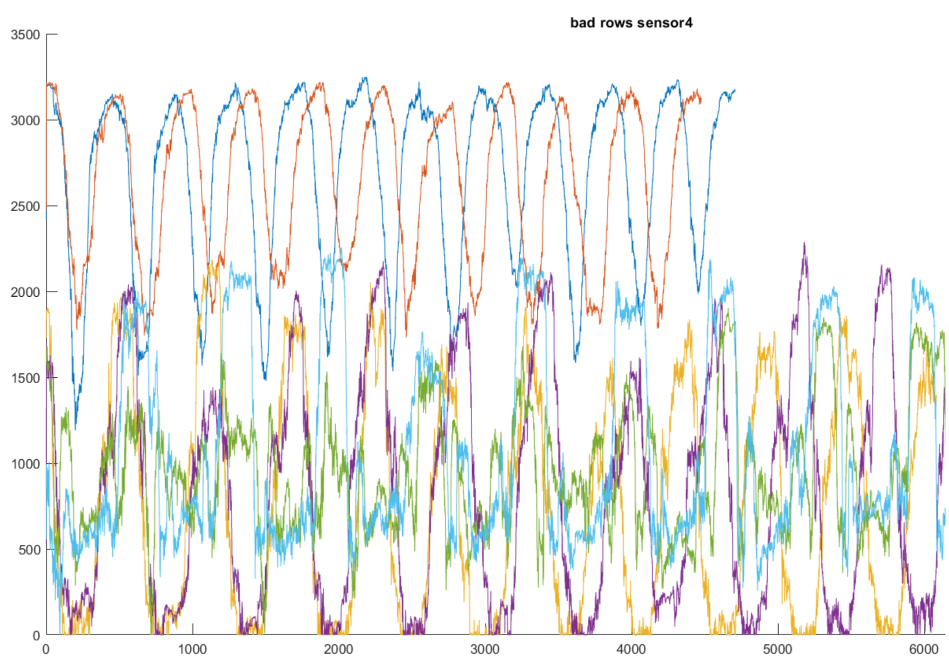

Figure 4.25: Readings from sensor 4 while doing rows with sub-optimal form. Each colour represents different sets. The X-axis represents the timescale and the Y-axis represents the analog sensor readings.

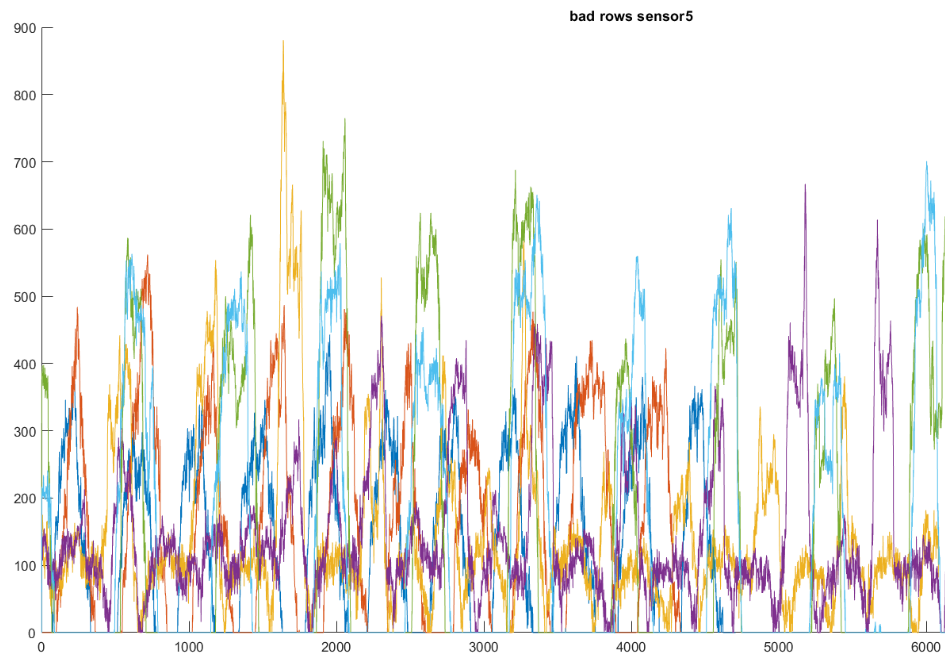

Figure 4.26: Readings from sensor 5 while doing rows with sub-optimal form. Each colour represents different sets. The X-axis represents the timescale and the Y-axis represents the analog sensor readings.

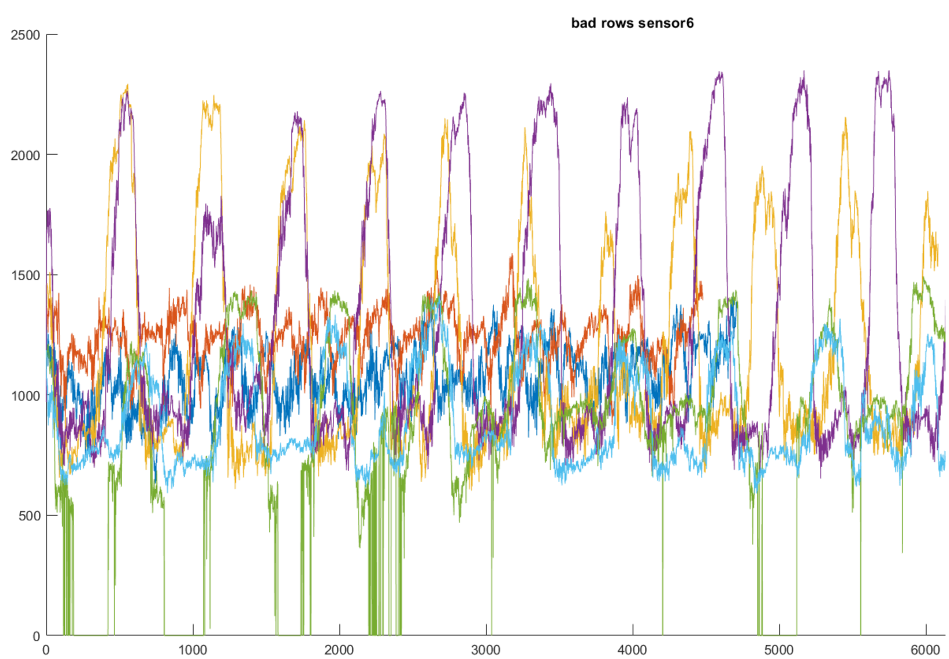

Figure 4.27: Readings from sensor 6 while doing rows with sub-optimal form. Each colour represents different sets. The X-axis represents the timescale and the Y-axis represents the analog sensor readings.

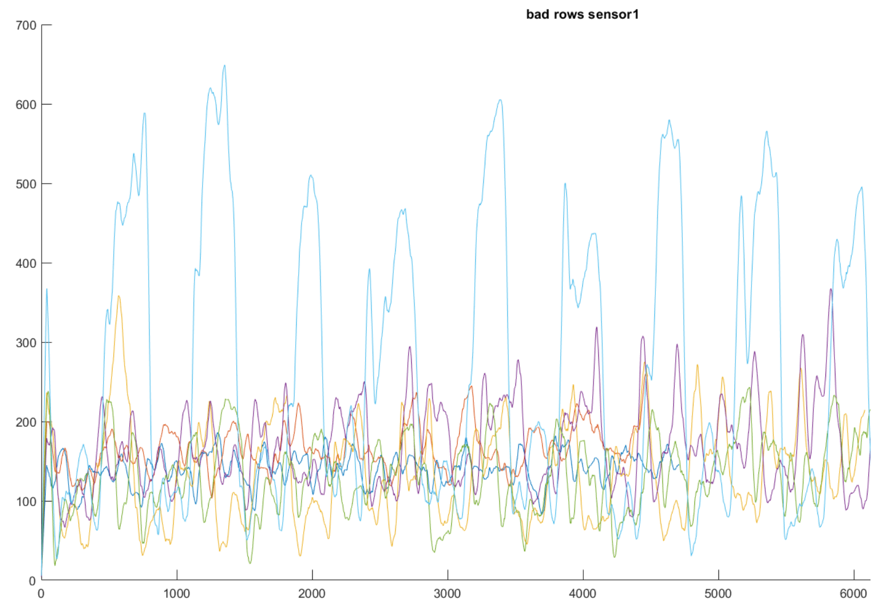

Figure 4.28: Readings from sensor 1 while doing rows with sub-optimal form after passing through a moving average filter. Each colour represents different sets. The X-axis represents the timescale and the Y-axis represents the analog sensor readings.

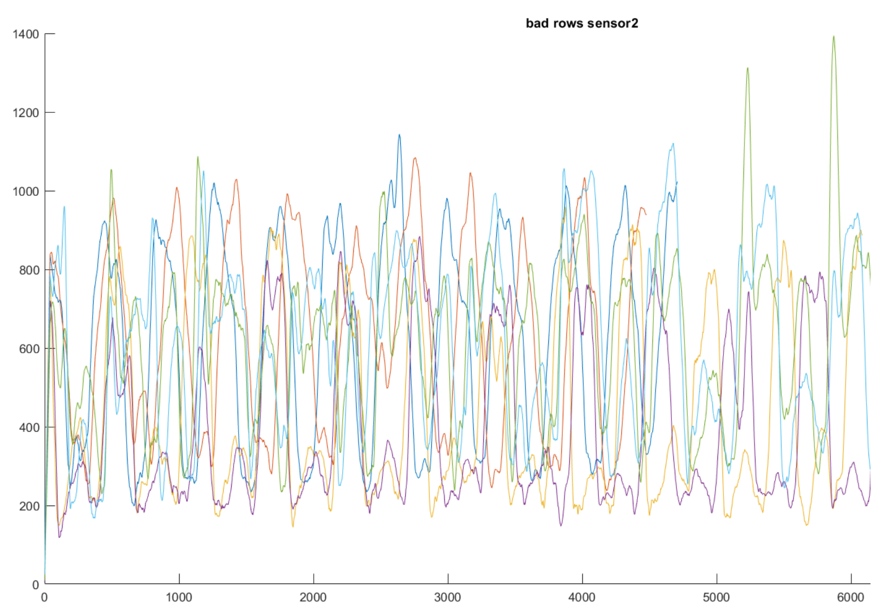

Figure 4.29: Readings from sensor 2 while doing rows with sub-optimal form after passing through a moving average filter. Each colour represents different sets. The X-axis represents the timescale and the Y-axis represents the analog sensor readings.

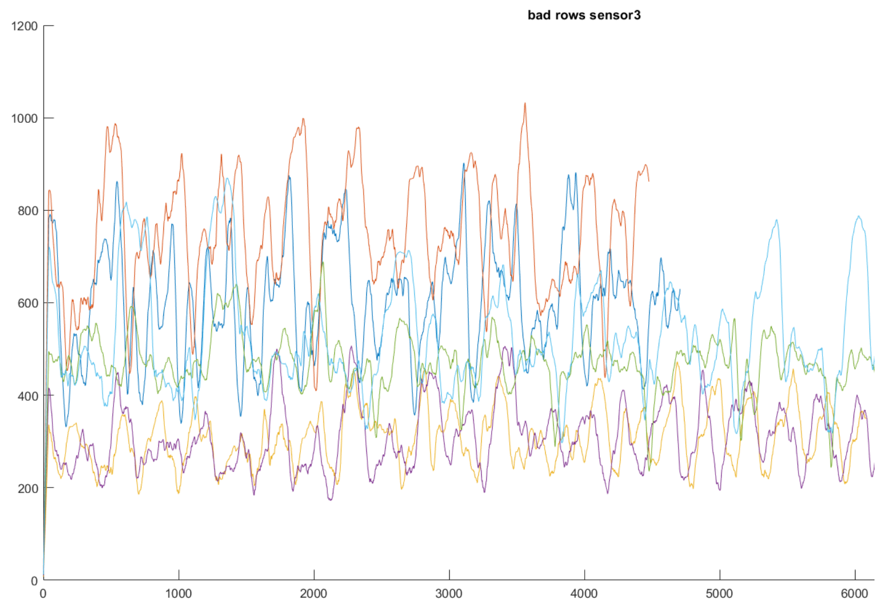

Figure 4.30: Readings from sensor 3 while doing rows with sub-optimal form after passing through a moving average filter. Each colour represents different sets. The X-axis represents the timescale and the Y-axis represents the analog sensor readings.

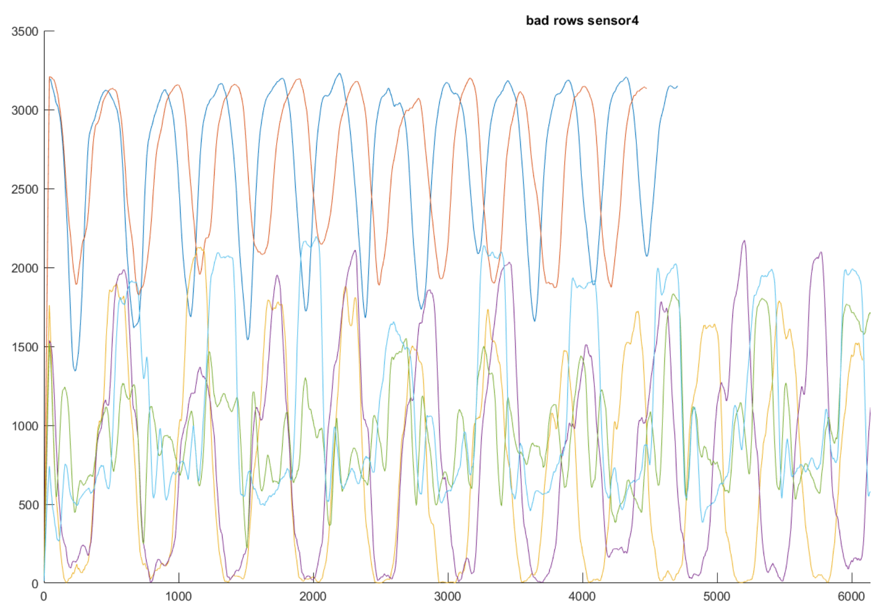

Figure 4.31: Readings from sensor 4 while doing rows with sub-optimal form after passing through a moving average filter. Each colour represents different sets. The X-axis represents the timescale and the Y-axis represents the analog sensor readings.

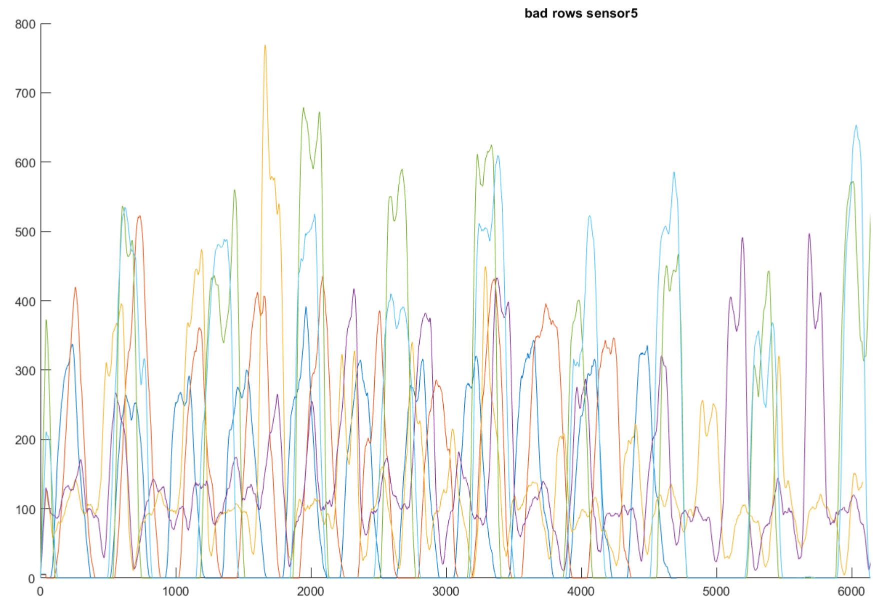

Figure 4.32: Readings from sensor 5 while doing rows with sub-optimal form after passing through a moving average filter. Each colour represents different sets. The X-axis represents the timescale and the Y-axis represents the analog sensor readings.

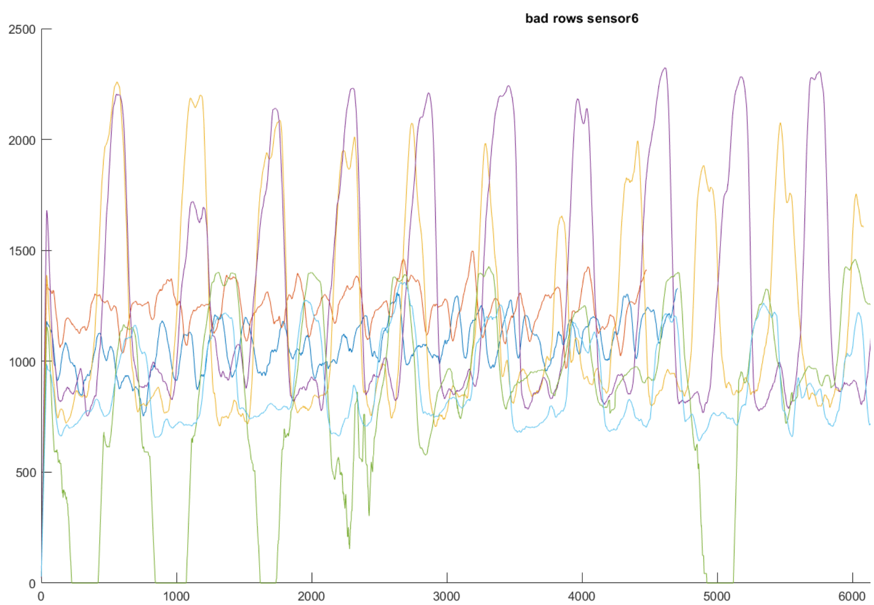

Figure 4.33: Readings from sensor 6 while doing rows with sub-optimal form after passing through a moving average filter. Each colour represents different sets. The X-axis represents the timescale and the Y-axis represents the analog sensor readings.

as num(false positive) - num(true positive) for all periods of 0.2 seconds. By iteratively adjusting the threshold value, our methodology aims to refine the accuracy of classification.

After thresholding, the five sensor data streams were combined into a single stream using the weighted sum of the values. The weight coefficients of each sensor are calculated based on the accuracy of feedback from each sensor. Sensors with a higher accuracy of prediction from the threshold are given higher weight. This is the same approach we have used in experiment one. Further details about the weighted sum can be found in previous sections.

The final step in the first check is to determine the threshold for our combined sensor stream. In the previous experiment, this value was based on the two least weights, reflecting the requirement for at least two of the five sensors to flag a repetition as bad. However, in the current experiment, designed as a 2-step check, we introduce a reduction in the threshold. This will reduce the false negatives but also reduce the accuracy. This reduction in accuracy is acceptable in light of the subsequent check that ensures a comprehensive and nuanced assessment of repetition quality.

4.3.3.2 Second check - Rate of Change analysis

The second check in our comprehensive analysis is dedicated to Rate of Change (RoC) analysis, refining the classification process initiated by the first check. The RoC analysis works best with a rep detector. This is a system that identifies when a rep is completed. This detector is based on the value when a user is standing normally. When a rep is detected, the smoothed rep reading is passed for the RoC analysis. The reading is passed through a differentiator to get the Rate of Change readings. This RoC readings encapsulates crucial information about the shape of the graph, contributing to a more nuanced understanding of the repetition dynamics, as explained in the previous sections.

The differentiated data is then subjected to thresholding by each sensor, providing individual verdicts on the RoC data. The process of determining the threshold is akin to our first check, involving the calculation of the mean peak values for both good and bad reps. Subsequently, a gradient descent method is applied to adjust the threshold value iteratively. Here also the loss function is taken as num(false positive) - num(true positive) for all periods of 0.2 seconds. By iteratively adjusting the threshold value, the accuracy of the classification improves. After thresholding, the five sensor data streams were combined into a single stream using the weighted sum of the values. The weight coefficients are determined based on the accuracy of feedback from each sensor, employing a methodology consistent with our approach in the previous experiment. This weighted sum ensures that sensors with a higher prediction accuracy hold more influence in the final verdict, a technique proven effective in our prior analysis. Next, we calculate the threshold for our combined sensor stream.

Now we have verdict from both the checks, the peak value check (D1) and the RoC check (D2). Both these verdicts are combined to give the final verdict. This final verdict is a simple weighted sum of D1 and D2 and a threshold to give the final decision. The weights are calculated based on the decision. The weight came out to be 0.67 for D2 and 0.33 for D1, which can be inferred as the accuracy of RoC analysis was double the accuracy of peak value analysis.

4.3.4 Results and discussion of experiment 2

Now that the analysis is explained, in this section we will be discussing the results. The Tables 4.2 4.3 4.4 shows each rep of each set of each subject doing rows. This figure gives a clear view of the accuracy of the output. The figure first shows how well the rep detection is working. Then the figure compares how the accuracy has changed after adding the RoC analysis. Tables 4.6 4.7 4.8 shows similar data for squats and Tables 4.10 4.11 4.12 for deadlifts. Table 4.5 shows all information about the accuracy. It shows the True Positive, True Negative, False Positive, and, False Negative. The Table shows all these details for analysis done without the RoC analysis and with it. It also shows the subject's accuracy information. Here S1, S2, S3 stands for subject 1, subject 2 and, subject 3. Table 4.9 shows similar data for squats and Table 4.13 for deadlifts.

Table 4.2: Rep-wise analysis for Rows. The table shows subject-wise decisions made by the rep detector

Set	Rep1	Rep2	Rep3	Rep4	Rep5	Rep6	Rep7	Rep8	Rep9	Rep10
S1 Bad1	1	1	1	1	1	1	1	1	1	1
S1 Bad2	1	1	1	1	1	1	1	1	1	1
S2 Bad1	1	1	1	1	1	1	1	1	1	1
S2 Bad2	1	1	1	1	1	1	1	1	1	1
S3 Bad1	0	1	1	1	1	1	1	1	1	1
S3 Bad2	1	1	1	1	1	1	1	1	1	1
S1 Good1	1	1	1	1	1	1	1	1	1	1
S1 Good2	1	1	1	1	1	1	1	1	1	1
S2 Good1	1	1	1	0	1	1	1	1	1	1
S2 Good2	1	1	1	1	1	1	1	1	1	1
S3 Good1	1	1	1	1	1	1	1	1	1	1
S3 Good2	1	1	1	0	0	1	1	0	1	1

Table 4.3: Rep-wise analysis for Rows. The table shows subject-wise decisions made by the peak analyzer

Set	Rep1	Rep2	Rep3	Rep4	Rep5	Rep6	Rep7	Rep8	Rep9	Rep10
S1 Bad1	1	0	1	1	1	0	0	0	1	1
S1 Bad2	0	0	0	0	1	0	0	0	0	0
S2 Bad1	1	1	1	1	1	1	1	1	1	1
S2 Bad2	1	1	1	1	1	1	1	1	1	1
S3 Bad1	1	1	1	1	1	1	0	1	1	1
S3 Bad2	0	1	1	1	1	1	1	1	1	1
S1 Good1	1	0	0	0	0	0	0	0	0	0
S1 Good2	0	0	0	0	0	0	0	0	0	0
S2 Good1	1	0	0	1	1	0	1	1	1	0
S2 Good2	0	1	1	1	1	1	1	1	1	0
S3 Good1	1	0	1	1	0	0	0	1	1	0
S3 Good2	1	0	1	0	0	0	0	0	1	1

Table 4.4: Rep-wise analysis for Rows. The table shows subject-wise decisions made by the RoC analyzer

Set	Rep1	Rep2	Rep3	Rep4	Rep5	Rep6	Rep7	Rep8	Rep9	Rep10
S1 Bad1	1	1	1	1	1	1	1	1	1	1
S1 Bad2	1	1	1	1	1	1	1	1	1	1
S2 Bad1	1	1	1	1	1	1	1	1	1	1
S2 Bad2	0	1	1	1	1	1	1	1	1	1
S3 Bad1	1	1	1	1	1	1	1	1	1	1
S3 Bad2	1	1	1	1	1	1	1	1	1	1
S1 Good1	0	1	0	0	0	0	0	0	0	1
S1 Good2	0	0	0	0	0	0	0	0	0	0
S2 Good1	0	0	0	0	0	0	0	0	0	0
S2 Good2	0	0	0	0	0	0	0	0	0	0
S3 Good1	0	0	0	0	0	0	0	0	0	0
S3 Good2	0	0	0	0	0	0	0	0	0	0

Table 4.5: subject-wise result for Rowing

			No RoC analysis			**with RoC analysis**		
	No Roc	***With RoC***	***S1***	***S2***	***S3***	***S1***	***S2***	***S3***
True Positive	45	59	7	20	18	20	19	20
True Negative	36	58	19	6	11	18	20	20
False Positive	24	2	1	14	9	2	0	0
False Negative	15	1	13	0	2	0	1	0

Table 4.6: Rep-wise analysis for Squats. The table shows subject-wise decisions made by the rep detector

Set	Rep1	Rep2	Rep3	Rep4	Rep5	Rep6	Rep7	Rep8	Rep9	Rep10
S1 Bad1	1	1	1	1	1	1	1	1	1	1
S1 Bad2	1	1	1	1	1	1	1	1	1	1
S2 Bad1	1	1	1	1	1	1	1	1	1	1
S2 Bad2	1	1	1	1	1	1	1	1	1	1
S3 Bad1	1	1	1	1	1	1	1	1	1	1
S3 Bad2	1	1	0	0	1	1	1	1	1	1
S1 Good1	1	1	1	1	1	1	1	1	1	1
S1 Good2	1	1	1	0	1	1	1	1	0	1
S2 Good1	0	1	1	0	1	1	1	1	1	1
S2 Good2	1	1	1	1	1	1	1	1	1	1
S3 Good1	1	1	1	1	1	1	1	1	1	1
S3 Good2	1	1	0	1	0	1	1	1	1	1

Table 4.7: Rep-wise analysis for Squats. The table shows subject-wise decisions made by the peak analyzer

Set	Rep1	Rep2	Rep3	Rep4	Rep5	Rep6	Rep7	Rep8	Rep9	Rep10
S1 Bad1	0	1	1	1	1	1	1	1	1	1
S1 Bad2	1	1	1	1	1	1	1	1	1	1
S2 Bad1	0	1	0	1	1	1	1	1	1	1
S2 Bad2	1	1	1	1	1	1	1	1	1	0
S3 Bad1	1	1	1	1	1	1	1	1	1	1
S3 Bad2	1	1	0	1	1	1	1	1	1	1
S1 Good1	0	0	0	0	0	1	1	0	0	0
S1 Good2	0	0	0	1	0	0	0	0	1	0
S2 Good1	0	0	0	0	0	0	0	0	0	0
S2 Good2	0	0	0	0	0	0	0	0	0	0
S3 Good1	0	0	0	0	0	0	0	0	0	0
S3 Good2	0	0	0	0	1	0	0	0	0	0

Table 4.8: Rep-wise analysis for Squats. The table shows subject-wise decisions made by the RoC analyzer

Set	Rep1	Rep2	Rep3	Rep4	Rep5	Rep6	Rep7	Rep8	Rep9	Rep10
S1 Bad1	1	1	1	1	1	1	1	1	1	1
S1 Bad2	1	1	1	1	1	1	1	1	1	1
S2 Bad1	1	1	1	1	1	1	1	1	1	1
S2 Bad2	1	1	1	1	1	1	1	1	1	1
S3 Bad1	1	1	1	1	1	1	1	1	1	1
S3 Bad2	1	1	1	1	1	1	1	1	1	1
S1 Good1	0	0	0	0	0	0	0	0	0	0
S1 Good2	0	0	0	0	0	0	0	0	0	0
S2 Good1	0	0	0	0	0	0	0	0	0	0
S2 Good2	0	0	0	0	0	0	0	0	0	0
S3 Good1	0	0	1	0	0	0	0	0	0	0
S3 Good2	0	0	0	1	0	0	0	0	0	0

Table 4.9: subject-wise result for Squats

			No RoC analysis			**with RoC analysis**		
	No Roc	***With RoC***	***S1***	***S2***	***S3***	***S1***	***S2***	***S3***
True Positive	55	60	19	17	19	20	20	20
True Negative	55	58	16	20	19	20	20	20
False Positive	5	2	4	0	1	0	0	2
False Negative	5	0	1	3	1	0	0	0

Table 4.10: Rep-wise analysis for Deadlifts. The table shows subject-wise decisions made by the rep detector

Set	Rep1	Rep2	Rep3	Rep4	Rep5	Rep6	Rep7	Rep8	Rep9	Rep10
S1 Bad1	1	1	1	1	1	1	1	1	1	1
S1 Bad2	1	1	1	1	1	1	1	1	1	1
S2 Bad1	1	1	1	1	1	1	1	1	1	1
S2 Bad2	1	1	1	1	1	1	1	1	1	1
S3 Bad1	1	0	1	1	1	1	1	1	1	1
S3 Bad2	1	1	0	1	1	1	1	1	1	1
S3 Bad3	0	0	1	1	1	1	1	1	1	1
S1 Good1	1	1	1	1	1	1	1	1	1	1
S1 Good2	1	1	0	1	1	1	1	1	1	1
S2 Good1	0	1	1	1	1	1	1	1	1	1
S2 Good2	1	1	1	1	1	1	1	1	1	1
S3 Good1	1	1	1	1	1	1	1	1	1	1
S3 Good2	1	1	1	1	1	1	1	1	1	1
S3 Good3	0	1	1	1	1	1	1	1	1	1

Table 4.11: Rep-wise analysis for Deadlifts. The table shows subject-wise decisions made by the peak analyser

Set	Rep1	Rep2	Rep3	Rep4	Rep5	Rep6	Rep7	Rep8	Rep9	Rep10
S1 Bad1	1	1	1	1	1	1	1	1	1	1
S1 Bad2	1	1	1	1	1	1	1	1	1	1
S2 Bad1	1	1	1	1	1	1	1	1	1	1
S2 Bad2	1	1	1	1	1	1	1	1	1	1
S3 Bad1	1	1	1	1	1	1	1	1	1	1
S3 Bad2	1	1	1	1	1	1	1	1	1	1
S3 Bad3	1	1	1	1	1	1	1	1	1	1
S1 Good1	0	1	0	0	1	0	0	0	0	0
S1 Good2	0	1	0	1	0	0	0	0	0	0
S2 Good1	0	0	1	0	0	1	1	0	0	0
S2 Good2	0	0	1	0	0	0	0	1	0	0
S3 Good1	1	0	0	1	0	1	0	0	0	0
S3 Good2	1	0	0	1	0	1	0	1	0	0
S3 Good3	0	0	1	1	0	0	0	0	0	0

Table 4.12: Rep-wise analysis for Deadlifts. The table shows subject-wise decisions made by the RoC analyzer

Set	Rep1	Rep2	Rep3	Rep4	Rep5	Rep6	Rep7	Rep8	Rep9	Rep10
S1 Bad1	1	1	1	1	1	1	1	1	1	1
S1 Bad2	1	1	1	1	1	1	1	1	1	1
S2 Bad1	1	1	1	1	1	1	1	1	1	1
S2 Bad2	1	1	1	1	1	1	1	1	1	1
S3 Bad1	1	1	1	1	1	1	1	1	1	1
S3 Bad2	1	1	1	1	1	1	1	1	1	1
S3 Bad3	1	1	1	1	1	1	1	1	1	1
S1 Good1	0	0	0	0	0	0	1	0	0	0
S1 Good2	0	0	0	0	1	0	0	0	0	0
S2 Good1	0	1	0	0	0	1	0	0	0	0
S2 Good2	0	0	1	0	0	0	0	0	0	1
S3 Good1	0	0	0	0	0	1	0	0	0	0
S3 Good2	0	0	0	0	0	0	1	0	0	0
S3 Good3	0	0	1	1	0	0	0	0	0	0

Table 4.13: subject-wise result for Deadlift

			No RoC analysis			**with RoC analysis**		
	No Roc	***With RoC***	***S1***	***S2***	***S3***	***S1***	***S2***	***S3***
True Positive	70	70	20	20	30	20	20	30
True Negative	52	60	16	15	21	18	17	26
False Positive	18	10	4	5	9	2	3	4
False Negative	0	0	0	0	0	0	0	0

Chapter 5

Conclusion

As a part of this dissertation, we presented the design and fabrication of a Wearable Pressure Sensor Suit for Real-Time Detection of Incorrect Exercise Techniques using a piezoresistive material, velostat, as the pressure-sensing element. The first experiment was done on deadlifts with classification done based on the peak value analysis. The experiment gave an accuracy of 100% in identifying good reps and a 90% accuracy in distinguishing bad reps. We quickly realized that person-to-person is not something scalable. So we tested on 2 other subjects using the first subject's calibration. The result was very positive, with an accuracy of 95%.

We did our next experiment with 3 exercises - deadlift, squat, and rows. We used a 2-step classification process to improve the quality of the result. The first step is the peak-value classification, and the next step is a 'Rate of Change' analysis. This analysis will help us incorporate information about the shape of the sensor readings. This will not just improve our accuracy but it will reduce the need for person-wise calibration further. The accuracy of the analysis for squats is 98%, the accuracy for deadlifts is 96%, and, the accuracy for rows is 96%.

5.0.1 Future Works

Presently, the suit's verdict system primarily relies on monitoring the posture of the back muscles. However, to augment its utility and provide a more comprehensive assessment, we plan to extend its capabilities to include verdicts based on other critical muscle groups such as the chest, shoulders, glutes, and more. By incorporating multi-dimensional feedback from various muscle groups, the suit will offer a more holistic evaluation of an individual's exercise form, thereby enhancing its effectiveness as a tool for optimizing workouts and preventing injuries.

A pivotal future milestone in the evolution of the suit is its integration with a dedicated mobile application. This innovative feature will facilitate seamless connectivity between the suit and the user's smartphone or tablet, enabling real-time data transmission and analysis. By leveraging the power of mobile technology, users will gain access to a wealth of features including logging and tracking of their workout progress, personalized recommendations for improvement, and even real-time alerts for improper form during exercises. This wireless connection not only enhances user convenience but also promotes accountability and motivation in achieving fitness goals.

In addition to its current focus on specific exercises such as deadlifts, squats, and rows, our vision for the suit encompasses broader functionality that extends to tracking a diverse range of exercises. Whether it's cardiovascular activities like running and cycling, or resistance training exercises targeting different muscle groups, the suit will be equipped with the capability to accurately monitor and assess form across various workout routines. This versatility ensures that users can benefit from the suit's feedback and guidance across their entire fitness regimen, promoting consistency and effectiveness in achieving their fitness objectives.

Chapter 6

Related Publications

- I. Kuriakose, S. Chauhan, A. Fatema and A. M. Hussain, ”Wearable Pressure Sensor Suit for Real-Time Detection of Incorrect Exercise Techniques,” 2022 IEEE Sensors, Dallas, TX, USA, 2022.

- A. Fatema, I. Kuriakose, R. Gupta and A. M. Hussain, ”Analysis of Interpolation Techniques for a Flexible Sensor Mat for Plantar Pressure Measurement,” 2023 IEEE Applied Sensing Conference (APSCON), Bengaluru, India, 2023.

- A. Fatema, I. Kuriakose, D. Devendra and A. M. Hussain, ”Investigation of the Mechanical Reliability of a Velostat-based Flexible Pressure Sensor,” 2022 IEEE International Conference on Flexible and Printable Sensors and Systems (FLEPS), Vienna, Austria, 2022, pp. 1-4.

Other Publications

- Datta Gupta, M., Mishra, R.B., Kuriakose, I. and Hussain, A.M., 2022. ”Determination of thermal and mechanical properties of SU-8 using electrothermal actuators.” MRS Advances, 7(28), pp.591-595.

- S. Chauhan, A. Fatema, I. Kuriakose and A. M. Hussain, ”Efficient Calibration of Velostat-Based Flexible Pressure Sensor Matrix,” 2023 IEEE International Conference on Flexible and Printable Sensors and Systems (FLEPS), Boston, MA, USA, 2023, pp. 1-4.

Appendix A

Codes

A.0.1 Arduino code to extract the sensor reading

```
const int sensor1 = 34;
const int sensor2 = 35;
const int sensor3 = 32;
const int sensor4 = 33;
const int sensor5 = 25;
const int sensor6 = 26;
const int sensor7 = 27;

int right_top = 0;
int left_bottom = 0;
int left_top = 0;
int left_middle = 0;
int centre = 0;
int right_middle = 0;
int right_bottom = 0;

void setup() {
  Serial.begin(115200);
  delay(1000);
}

void loop() {
  left_bottom = analogRead(sensor1);//left bottom
  right_top = analogRead(sensor2); // right top
  right_bottom = analogRead(sensor3);//right bottom
  right_middle = analogRead(sensor4);//right middle
  centre = analogRead(sensor5);
  left_middle = analogRead(sensor6);//left middle
  left_top = analogRead(sensor7);//left top

```

```
  Serial.print(right_top);Serial.print(",");
  Serial.print(left_top);Serial.print(",");
  Serial.print(right_middle);Serial.print(",");
  Serial.print(left_middle);Serial.print(",");
  Serial.print(right_bottom);Serial.print(",");
  Serial.print(left_bottom);Serial.print(",");
  Serial.print(centre);Serial.print(",");
  Serial.println();
  delay(10);
}

```

A.0.2 Python code to load the Arduino output to a text file

```python
import tkinter
import serial
import numpy as np; np.random.seed(0)
import matplotlib.pyplot as plt
import datetime

ser = serial.Serial('COM5', 9600)
top = tkinter.Tk()
top.geometry("200x200")

last_received = ''
buffer_string = ''

def read_sensor():
    global last_received
    global buffer_string
    buffer_string = buffer_string + ser.read(ser.inWaiting()).decode('ascii')
    if '\n' in buffer_string:
        lines = buffer_string.split('\n')
        last_received = lines[-2]
        buffer_string = lines[-1]

    if last_received != '':
        X1= last_received[:-2]
        arr2 = X1.split(",")
        arr=[]
        for i in arr2:
            arr.append(float(i))

    reading_string = "\n"
```

```
    reading_string+=str(datetime.datetime.now())
    reading_string+=","
    reading_string+=str(arr[0])
    reading_string+=","
    reading_string+=str(arr[1])
    reading_string+=","
    reading_string+=str(arr[2])
    reading_string+=","
    reading_string+=str(arr[3])
    reading_string+=","
    reading_string+=str(arr[4])
    reading_string+=","
    reading_string+=str(arr[5])

    file1 = open("ivin-recalib-gooddeadlift2.txt", "a")
    file1.write(reading_string)
    file1.close()

def loop(toggle=False):
    global tracking_var
    if toggle:
        if tracking_var:
            tracking_var = False
        else:
            tracking_var = True

    if tracking_var:
        read_sensor()
        top.after(10, loop)
    else:
      plt.close()

tracking_var = False
B = tkinter.Button(top, text ="Go!", command=lambda: loop(True))

B.pack()
top.eval('tk::PlaceWindow . center')
top.mainloop()
ser.close()
```

Bibliography

[1] Thomas R Baechle and Roger W Earle. *Weight training: steps to success*. Human Kinetics, 2019.

[2] Pamela A Williams and Thomas F Cash. Effects of a circuit weight training program on the body images of college students. *Int. J. Eat. Disord.*, 30(1):75–82, 2001.

[3] William J Kraemer, Nicholas A Ratamess, and Duncan N French. Resistance training for health and performance. *Curr. Sports Med. Rep.*, 1(3):165–171, 2002.

[4] Greg J Wilson, Aron J Murphy, and Andrew Walshe. The specificity of strength training: the effect of posture. *Eur. J. Appl. Physiol.*, 73(3):346–352, 1996.

[5] Justin WL Keogh and Paul W Winwood. The epidemiology of injuries across the weight-training sports. *Sports Med.*, 47(3):479–501, 2017.

[6] Victor Bengtsson, Lars Berglund, and Ulrika Aasa. Narrative review of injuries in powerlifting with special reference to their association to the squat, bench press and deadlift. *BMJ Open Sport Exerc. Med.*, 4(1):e000382, 2018.

[7] David A Connell, Hollis G Potter, Mark F Sherman, and Thomas L Wickiewicz. Injuries of the pectoralis major muscle: evaluation with mr imaging. *Radiology*, 210(3):785–791, 1999.

[8] Sakari Orava and Urho M Kujala. Rupture of the ischial origin of the hamstring muscles. *The American Journal of Sports Medicine*, 23(6):702–705, 1995.

[9] Thomas A Brady, Bernard R Cahill, and Leslie M Bodnar. Weight training-related injuries in the high school athlete. *Am. J. Sports Med.*, 10(1):1–5, 1982.

[10] Rejean Grenier and Andre Guimont. Simultaneous bilateral rupture of the quadriceps tendon and leg fractures in a weightlifter: a case report. *Am. J. Sports Med.*, 11(6):451–453, 1983.

[11] Edit Strömbäck, Ulrika Aasa, Kajsa Gilenstam, and Lars Berglund. Prevalence and consequences of injuries in powerlifting: A cross-sectional study. *Orthop. J. Sports Med.*, 6(5):2325967118771016, 2018.

[12] Sherjeel M Khan, Nadeem Qaiser, Sohail F Shaikh, and Muhammad Mustafa Hussain. Design analysis and human tests of foil-based wheezing monitoring system for asthma detection. *IEEE Trans. Electron Devices*, 67(1):249–257, 2019.

[13] Aftab M Hussain. *Introduction to Flexible Electronics*. CRC Press, 2022.

[14] Club Intel. The U.S. Member Journey in the Era of Covid-19. [Online]. Available: `https://www.club-intel.com/wp-content/uploads/Final-The-Member-Journey-in-the-Era-of-Covid-19.pdf`.

[15] Karina Sokolova and Charles Perez. You follow fitness influencers on youtube. but do you actually exercise? how parasocial relationships, and watching fitness influencers, relate to intentions to exercise. *Journal of retailing and consumer services*, 58:102276, 2021.

[16] Rodrigo Luiz Vancini, Ricardo Borges Viana, Marilia dos Santos Andrade, Claudio Andre Barbosa de Lira, Pantelis Theodoros Nikolaidis, Alexandre Aparecido de Almeida, and Beat Knechtle. Youtube as a source of information about physical exercise during covid-19 outbreak. *International Journal of Sport Studies for Health*, 4(2):e123312, 2022.

[17] Suputtra Sutthiprapa, Vajirasak Vanijja, and Thanakrit Likitwon. The deadlift form analysis system using microsoft kinect. *Procedia Comput. Sci.*, 111:174–182, 2017.

[18] Chen-Yi Lin and Kuan-Cheng Jian. A real-time algorithm for weight training detection and correction. *Soft Comput.*, 26(10):4727–4739, 2022.

[19] Isabelle Poitras, Frédérique Dupuis, Mathieu Bielmann, Alexandre Campeau-Lecours, Catherine Mercier, Laurent J Bouyer, and Jean-Sébastien Roy. Validity and reliability of wearable sensors for joint angle estimation: A systematic review. *Sens.*, 19(7):1555, 2019.

[20] Zhelong Wang, Ruichen Liu, Hongyu Zhao, Sen Qiu, Xin Shi, Jiaxin Wang, and Jie Li. Motion analysis of deadlift for trainers with different levels based on body sensor network. *IEEE Trans. Instrum. Meas.*, 70:1–12, 2021.

[21] Florian Michaud, Manuel Pérez Soto, Urbano Lugrís, and Javier Cuadrado. Lower back injury prevention and sensitization of hip hinge with neutral spine using wearable sensors during lifting exercises. *Sens.*, 21(16):5487, 2021.

[22] Kevin Jeulink. Smart sports exercises project: the detection of (in) correct motion during resistance training. B.S. thesis, University of Twente, 2020.

[23] Jorge E Caviedes, Baoxin Li, and Varun C Jammula. Wearable sensor array design for spine posture monitoring during exercise incorporating biofeedback. *IEEE. Trans. Biomed. Eng.*, 67(10):2828–2838, 2020.

[24] Abdul Hannan, Muhammad Zohaib Shafiq, Faisal Hussain, and Ivan Miguel Pires. A portable smart fitness suite for real-time exercise monitoring and posture correction. *Sens.*, 21(19):6692, 2021.

[25] Francesco Felici and Alessandro Del Vecchio. Surface electromyography: what limits its use in exercise and sport physiology? *Front. Neurol.*, 11:578504, 2020.

[26] Chang-Ming Yang, Tsu-Lin Yang, Wen-Tzeng Huang, Chin-Hsing Chen, Shu-Hui Hung, Chih-Ming Cheng, and Mu-Huo Cheng. A novel design and evaluation of wearable digital sensor for monitoring posture. In *2008 30th Annual International Conference of the IEEE Engineering in Medicine and Biology Society*, pages 1304–1307. IEEE, 2008.

[27] Amit Nagarkoti, Revant Teotia, Amith K Mahale, and Pankaj K Das. Realtime indoor workout analysis using machine learning & computer vision. In *2019 41st Annual international conference of the IEEE engineering in medicine and biology society (EMBC)*, pages 1440–1443. IEEE, 2019.

[28] Ze Wu, Jiwen Zhang, Ken Chen, and Chenglong Fu. Yoga posture recognition and quantitative evaluation with wearable sensors based on two-stage classifier and prior bayesian network. *Sensors*, 19(23):5129, 2019.

[29] Xiaoou Li, Zhiyong Zhou, Jiajia Wu, and Yichao Xiong. Human posture detection method based on wearable devices. *Journal of healthcare engineering*, 2021(1):8879061, 2021.

[30] Amir Nadeem, Ahmad Jalal, and Kibum Kim. Automatic human posture estimation for sport activity recognition with robust body parts detection and entropy markov model. *Multimedia Tools and Applications*, 80:21465–21498, 2021.

[31] Anis Fatema, Surya Poondla, Rishabh B. Mishra, and Aftab M. Hussain. A Low-Cost Pressure Sensor Matrix for Activity Monitoring in Stroke Patients Using Artificial Intelligence. *IEEE Sens. J.*, 21(7):9546–9552, 2021.

[32] Alejandro Perdomo-Campos, Iliover Vega-González, and Jorge Ramirez-Beltran. Esp32 based low-power and low-cost wireless sensor network. In *The conference on Latin America Control Congress*, pages 275–285. Springer, 2020.

[33] M Cakmak, M Hassan, E Unsal, and C Martins. A fast real time measurement system to track in and out of plane optical retardation/birefringence, true stress, and true strain during biaxial stretching of polymer films. *Review of Scientific Instruments*, 83(12), 2012.

[34] Etienne Lemaire, Renaud Moser, CJ Borsa, and Danick Briand. Green paper-based piezoelectronics for sensors and actuators. *Sens. Actuator A: Phys.*, 244:285–291, 2016.

[35] Sherjeel M Khan, RB Mishra, Nadeem Qaiser, Aftab M Hussain, and Muhammad Mustafa Hussain. Diaphragm shape effect on the performance of foil-based capacitive pressure sensors. *AIP Adv.*, 10(1):015009, 2020.

[36] Darren J Lipomi, Michael Vosgueritchian, Benjamin CK Tee, Sondra L Hellstrom, Jennifer A Lee, Courtney H Fox, and Zhenan Bao. Skin-like pressure and strain sensors based on transparent elastic films of carbon nanotubes. *Nat. Nanotechnol.*, 6(12):788–792, 2011.

[37] Rishabh Bhooshan Mishra, Seshadri Reddy Nagireddy, Sumana Bhattacharjee, and Aftab M Hussain. Theoretical modeling and numerical simulation of elliptical capacitive pressure microsensor. In *2019 IEEE Conference on Modeling of Systems Circuits and Devices (MOS-AK India)*, pages 17–22. IEEE, 2019.

[38] Rishabh B Mishra, Sherjeel M Khan, Sohail F Shaikh, Aftab M Hussain, and Muhammad M Hussain. Low-cost foil/paper based touch mode pressure sensing element as artificial skin module for prosthetic hand. In *2020 3rd IEEE International Conference on Soft Robotics (RoboSoft)*, pages 194–200. IEEE, 2020.

[39] Rishabh B Mishra, Nazek El-Atab, Aftab M Hussain, and Muhammad M Hussain. Recent progress on flexible capacitive pressure sensors: From design and materials to applications. *Adv. Mater. Technol.*, 6(4):2001023, 2021.

[40] Fenlan Xu, Xiuyan Li, Yue Shi, Luhai Li, Wei Wang, Liang He, and Ruping Liu. Recent developments for flexible pressure sensors: A review. *Micromachines*, 9(11):580, 2018.

[41] Morito Akiyama, Yukari Morofuji, Toshihiro Kamohara, Keiko Nishikubo, Masayoshi Tsubai, Osamu Fukuda, and Naohiro Ueno. Flexible piezoelectric pressure sensors using oriented aluminum nitride thin films prepared on polyethylene terephthalate films. *Journal of applied physics*, 100(11):114318, 2006.

[42] Gustav Gautschi. Piezoelectric sensors. In *Piezoelectric Sensorics*, pages 73–91. Springer, 2002.

[43] Leonardo Martins, Rui Lucena, João Belo, Rui Almeida, Cláudia Quaresma, Adelaide P Jesus, and Pedro Vieira. Intelligent chair sensor–classification and correction of sitting posture. In *XIII Mediterranean Conference on Medical and Biological Engineering and Computing 2013*, pages 1489–1492. Springer, 2014.

[44] DDL Chung. A critical review of piezoresistivity and its application in electrical-resistance-based strain sensing. *Journal of Materials Science*, 55(32):15367–15396, 2020.

[45] RB Mishra, Sohail F Shaikh, Aftab M Hussain, and Muhammad Mustafa Hussain. Metal coated polymer and paper-based cantilever design and analysis for acoustic pressure sensing. *Aip Adv.*, 10(5):055112, 2020.

[46] Davide Giovanelli and Elisabetta Farella. Force sensing resistor and evaluation of technology for wearable body pressure sensing. *Journal of Sensors*, 2016, 2016.

[47] Suhan Muppavram, Nipoon Patel, and Muhammad Nadeem. Posture alert. In *2018 IEEE Region Ten Symposium (Tensymp)*, pages 213–218. IEEE, 2018.

[48] SS Suprapto, AW Setiawan, H Zakaria, W Adiprawita, and B Supartono. Low-cost pressure sensor matrix using velostat. In *2017 5th International Conference on Instrumentation, Communications, Information Technology, and Biomedical Engineering (ICICI-BME)*, pages 137–140. IEEE, 2017.

[49] Liangqi Yuan, Hongwei Qu, and Jia Li. Velostat sensor array for object recognition. *IEEE Sensors Journal*, 22(2):1692–1704, 2022.

[50] Eunseok Jeong, Jaehong Lee, and DaeEun Kim. Finger-gesture recognition glove using velostat (iccas 2011). In *2011 11th International Conference on Control, Automation and Systems*, pages 206–210. IEEE, 2011.

[51] Rik van Donselaar and Wei Chen. Design of a smart textile mat to study pressure distribution on multiple foam material configurations. In *Proceedings of the 4th International Symposium on Applied Sciences in Biomedical and Communication Technologies*, pages 1–5, 2011.

[52] Haris Muhedinovic and Dusanka Boskovic. Design of iot solution for velostat footprint pressure sensor system. In *International Conference on IoT Technologies for HealthCare*, pages 171–176. Springer, 2016.

[53] Matthew Hopkins, Ravi Vaidyanathan, and Alison H Mcgregor. Examination of the performance characteristics of velostat as an in-socket pressure sensor. *IEEE Sensors Journal*, 20(13):6992–7000, 2020.

[54] Hannah Perner-Wilson and Mika Satomi. Diy wearable technology. In *ISEA 15th International Symposium on Electronic Art*, 2009.

[55] Laurel S Pardue, Christopher Harte, and Andrew P McPherson. A low-cost real-time tracking system for violin. *Journal of New Music Research*, 44(4):305–323, 2015.

[56] Anis Fatema, Surya Poondla, Rishabh B. Mishra, and Aftab M. Hussain. A low-cost pressure sensor matrix for activity monitoring in stroke patients using artificial intelligence. *IEEE Sensors Journal*, 21(7):9546–9552, 2021.

[57] Z Del Prete, L Monteleone, and R Steindler. A novel pressure array sensor based on contact resistance variation: Metrological properties. *Review of Scientific Instruments*, 72(2):1548–1553, 2001.

[58] Mathias Sundholm, Jingyuan Cheng, Bo Zhou, Akash Sethi, and Paul Lukowicz. Smart-mat: Recognizing and counting gym exercises with low-cost resistive pressure sensing matrix. In *Proceedings of the 2014 ACM international joint conference on pervasive and ubiquitous computing*, pages 373–382, 2014.

[59] Michal Gála, Ján Barabáš, and Mariana Kopásková. User presence monitoring based on velostat pressure sensors and arduino platform. In *2020 IEEE 21st International Conference on Computational Problems of Electrical Engineering (CPEE)*, pages 1–3. IEEE, 2020.

[60] Anis Fatema, Shirley Chauhan, Mohee Datta Gupta, and Aftab M. Hussain. Investigation of the long-term reliability of a velostat-based flexible pressure sensor array for 210 days. *IEEE Transactions on Device and Materials Reliability*, 24(1):41–48, 2024.

[61] Shirley Chauhan, Anis Fatema, Ivin Kuriakose, and Aftab M. Hussain. Efficient calibration of velostat-based flexible pressure sensor matrix. In *2023 IEEE International Conference on Flexible and Printable Sensors and Systems (FLEPS)*, pages 1–4, 2023.

[62] Anis Fatema, Ivin Kuriakose, Deeksha Devendra, and Aftab M Hussain. Investigation of the mechanical reliability of a velostat-based flexible pressure sensor. In *2022 IEEE International Conference on Flexible and Printable Sensors and Systems (FLEPS)*, pages 1–4. IEEE, 2022.

[63] Mohee Datta Gupta, L. Lakshmanan, Anis Fatema, and Aftab M. Hussain. Flexible writing pad based on a piezoresistive thin film sensor matrix. In *2023 IEEE Applied Sensing Conference (APSCON)*, pages 1–3, 2023.

[64] Kevin Farley. Analysis of the conventional deadlift. *Strength Cond. J.*, 17:55–61, 1995.

[65] Stephen Bird and Benjamin Barrington-Higgs. Exploring the deadlift. *Strength & Conditioning Journal*, 32(2):46–51, 2010.

[66] Vishakha Pandey and VK Giri. High frequency noise removal from ecg using moving average filters. In *2016 International conference on emerging trends in electrical electronics & sustainable energy systems (ICETEESES)*, pages 191–195. IEEE, 2016.

[67] Saeed Golestan, Malek Ramezani, Josep M Guerrero, Francisco D Freijedo, and Mohammad Monfared. Moving average filter based phase-locked loops: Performance analysis and design guidelines. *IEEE Transactions on Power Electronics*, 29(6):2750–2763, 2013.

[68] José Luis Guiñón, Emma Ortega, José García-Antón, and Valentín Pérez-Herranz. Moving average and savitzki-golay smoothing filters using mathcad. *Papers ICEE*, 2007:1–4, 2007.

[69] Jinyu Wang, Jun Liang, Feng Gao, Li Zhang, and Zhuodi Wang. A method to improve the dynamic performance of moving average filter-based pll. *IEEE Transactions on Power Electronics*, 30(10):5978–5990, 2014.

[70] HC Chen and Szi-Wen Chen. A moving average based filtering system with its application to real-time qrs detection. In *Computers in Cardiology, 2003*, pages 585–588. IEEE, 2003.

[71] Tomasz Wiktorski and Aleksandra Królak. Extended approach to sum of absolute differences method for improved identification of periods in biomedical time series. *MethodsX*, 7:101094, 2020.

[72] Bowei Yan, Sanmi Koyejo, Kai Zhong, and Pradeep Ravikumar. Binary classification with karmic, threshold-quasi-concave metrics. In *International Conference on Machine Learning*, pages 5531–5540. PMLR, 2018.

[73] Elizabeth A Freeman and Gretchen G Moisen. A comparison of the performance of threshold criteria for binary classification in terms of predicted prevalence and kappa. *Ecological modelling*, 217(1-2):48–58, 2008.

[74] Oluwasanmi O Koyejo, Nagarajan Natarajan, Pradeep K Ravikumar, and Inderjit S Dhillon. Consistent binary classification with generalized performance metrics. *Advances in neural information processing systems*, 27, 2014.

[75] TF Smith, ZF Shen, and JN Friedman. Evaluation of coefficients for the weighted sum of gray gases model. 1982.

[76] Jonathan C Gullett, Mark D Tillman, Gregory M Gutierrez, and John W Chow. A biomechanical comparison of back and front squats in healthy trained individuals. *The Journal of Strength & Conditioning Research*, 23(1):284–292, 2009.

[77] Eric L Dugan, Tim LA Doyle, Brendan Humphries, Christopher J Hasson, and Robert U Newton. Determining the optimal load for jump squats: a review of methods and calculations. *The Journal of Strength & Conditioning Research*, 18(3):668–674, 2004.

[78] Irineu Loturco, Timothy Suchomel, Ronaldo Kobal, Ademir FS Arruda, Aristide Guerriero, Lucas A Pereira, and Chi N Pai. Force-velocity relationship in three different variations of prone row exercises. *The Journal of Strength & Conditioning Research*, 35(2):300–309, 2021.

[79] Peter Ronai. The barbell row exercise. *ACSM's Health & Fitness Journal*, 21(2):25–28, 2017.

[80] Paul Comfort and Peter Kasim. Optimizing squat technique. *Strength & Conditioning Journal*, 29(6):10–13, 2007.

[81] C Sidney Burrus and T Parks. Convolution algorithms. *Citeseer: New York, NY, USA*, 6:15, 1985.

[82] Eric W Weisstein. Convolution. *https://mathworld. wolfram. com/*, 2003.

[83] David Haussler et al. Convolution kernels on discrete structures. Technical report, Citeseer, 1999.

[84] Habibollah Agh Atabay. Binary shape classification using convolutional neural networks. *IIOAB J*, 7(5):332–336, 2016.

[85] Yunho Jeon and Junmo Kim. Active convolution: Learning the shape of convolution for image classification. In *Proceedings of the IEEE conference on computer vision and pattern recognition*, pages 4201–4209, 2017.

[86] Saad Albawi, Tareq Abed Mohammed, and Saad Al-Zawi. Understanding of a convolutional neural network. In *2017 international conference on engineering and technology (ICET)*, pages 1–6. Ieee, 2017.

[87] Jiuxiang Gu, Zhenhua Wang, Jason Kuen, Lianyang Ma, Amir Shahroudy, Bing Shuai, Ting Liu, Xingxing Wang, Gang Wang, Jianfei Cai, et al. Recent advances in convolutional neural networks. *Pattern recognition*, 77:354–377, 2018.

[88] Keiron O'shea and Ryan Nash. An introduction to convolutional neural networks. *arXiv preprint arXiv:1511.08458*, 2015.